R. & M. No. 3238

MINISTRY OF AVIATION

AERONAUTICAL RESEARCH COUNCIL
REPORTS AND MEMORANDA

The Pressure Distribution on Two-Dimensional Wings near the Ground

By J. A. Bagley, B.Sc.

LONDON: HER MAJESTY'S STATIONERY OFFICE
1961
PRICE SIXTEEN SHILLINGS NET

The Pressure Distribution on Two-Dimensional Wings near the Ground

By J. A. Bagley, B.Sc.

Communicated by the Deputy Controller Aircraft (Research and Development), Ministry of Aviation

*Reports and Memoranda No. 3238**
February, 1960

Summary. A simple method of calculating the pressure distribution in incompressible flow on two-dimensional aerofoils of arbitrary section at moderate distances from the ground is developed. Comparisons with an 'exact' potential-flow solution, and with measurements on a 10 per cent thick aerofoil of RAE 101 section, provide a satisfactory verification of the adequacy of the method; but it is shown that it is necessary to take account of the boundary layer on the aerofoil in the calculations.

1. *Introduction.* The changes in the aerodynamic characteristics of a wing as it approaches the ground have been investigated, both theoretically and experimentally, by many workers over a considerable period. For the most part, such investigations have been concerned only with the changes in the overall forces, and the detailed changes in the surface pressure distribution have had little practical interest and have therefore rarely been explicitly considered. However, in recent years it has become clear that, in certain circumstances, quite small changes in the surface pressure distribution can provoke substantial alterations in stalling behaviour for certain aerofoils which are close to the boundary between those which stall following boundary-layer separation near the nose, and those which stall in consequence of separation at the rear of the section[1]. The present work originated, therefore, in an attempt to assess whether a change in stalling behaviour might occur on a specific wing as it approached the ground; but in the present Report the more general problem is considered of predicting the pressures when the flow is attached, and only a few remarks are made about stalling behaviour.

It should be emphasised that only the two-dimensional problem is considered in this paper. On any finite wing, the major effect of the proximity of the ground is a reduction in downwash due to the displacement of the trailing vortices, leading to an increase in the effective incidence at a given geometrical incidence. The reduction in induced incidence can be expressed in the form

$$\Delta\alpha_i = \sigma \frac{C_L}{\pi A}.$$

Values of σ for elliptically-loaded wings were given by Prandtl in his classic work on biplanes, and values for the load distributions which give minimum induced drag were calculated by de Haller[2];

* Previously issued as R.A.E. Report Aero. No. 2625—A.R.C. 22,060.

the differences in value are usually of no practical significance. A number of authors have developed calculation methods for dealing with practical wings and complete aircraft: the differences between them are primarily in the choice of a representative point whose height above the ground is taken as the measure of ground proximity. This choice is conditioned by the particular selection of wing planforms which is significant at a particular moment of history (*see*, for example, Wood and Trebble[3]). A calculation method of somewhat greater generality has been developed by Licher[4] who represents the wing by a number of horseshoe vortices distributed over the wing planform.

Reverting to the two-dimensional aerofoil, the present method essentially follows that of Tani[5], who calculated the change in circulation around the aerofoil due to the proximity of the ground by replacing the aerofoil by a sum of three standard vortex distributions on the chord line (as in Birnbaum's classical treatment of the isolated aerofoil) together with their images in the ground plane. The strengths of the three standard distributions were determined by satisfying the boundary condition, that the aerofoil chord line should be a streamline, at three points. The effect of finite thickness of the wing was simulated by a single doublet together with its image in the ground plane. In this Report, essentially the same approach is followed: the major difference is the use of a distribution of sources along the aerofoil chord to represent the finite thickness of the wing. The images of these sources produce normal velocities at the aerofoil; thus an additional vortex distribution along the chord is required if the boundary condition is still to be satisfied. By using some tables of the velocity increments due to the three standard vortex distributions[6] on two parallel straight lines and a convenient numerical method of finding the velocities due to the sources, the calculation method is reduced to a simple and convenient form for practical use.

In principle, the two-dimensional flow about an aerofoil near the ground can be formulated as a problem in potential theory, and 'exact' solutions can be found by the use of conformal transformations. In this way Tomotika and various co-authors[7] obtained the solution for a flat plate, and de Haller[2] dealt independently with flat-plate and circular-arc aerofoils. Havelock[8], Green[9], Tomotika[10] and Fujikawa[11] have all considered aerofoils of finite thickness, but the solutions are always expressed in terms of the transformation coefficients: these are only obtained with considerable labour from the geometrical details of aerofoil shape, incidence and ground distance which define a practical case. A further difficulty, except in Ref. 10, is that the results are not given in closed form but as infinite series, so that although the solution is 'exact', the numerical accuracy of a particular example cannot be guaranteed until the convergence of the series has been investigated. Such methods are thus not at all convenient for the calculation of pressure distributions on arbitrary aerofoil sections; although it might be feasible to adapt them for use with high-speed digital computing machinery, it seems questionable whether the programming effort needed would be justifiable as long as adequate results can be obtained from simpler methods such as the present one. In any case, it appears from the present work that viscous effects would have to be included if any improvement on the method given here were to be obtained.

The exact solution obtained for a particular aerofoil section by Tomotika[10] is used in Section 2.4 as a check on the present approximate method, which shows that the approximations made are acceptable within potential theory. To discover the significance of viscous effects, a comparison with experimental results is needed. As no experimental results of sufficient accuracy were available, tests were made in the No. 2 $11\frac{1}{2}$ ft $\times$ $8\frac{1}{2}$ ft Low-Speed Wind Tunnel at the Royal Aircraft Establishment, Farnborough; these are described in Section 3. These tests were made on an aerofoil with a thickness/chord ratio of 10 per cent, using a solid reflection plate to simulate the ground.

This technique has frequently been criticised as an unrealistic representation of the practical case, but it is believed that the modification of the standard method used here is satisfactory.

The comparison between the experimental and theoretical results is presented in Section 4. It is found that the effect of the aerofoil boundary layer has to be taken into account in calculating the theoretical pressure distribution, as was previously found for the isolated aerofoil by Brebner and Bagley[12]. At present, it is not possible to calculate the boundary-layer development entirely by theoretical methods, but it is shown in Section 4 that once the boundary layer is known, its effect can be included in the calculations, which then agree very well with the experiments.

2. *Theoretical Calculation of the Velocity Distribution.* 2.1. *Basis of Calculation.* The calculation method developed in this note is based closely on Weber's treatment[13, 14] of the isolated two-dimensional aerofoil. Distributions of sources and vortices are used to represent the aerofoil thickness and circulation respectively, and the effect of the ground is reproduced by considering the influence of the images of these singularities in the ground plane.

A co-ordinate system is used where x is measured along the wing chord and z vertically upwards from an origin at the aerofoil nose. The free-stream velocity is V_0 with components V_{x0} and V_{z0}; the velocity increments due to the singularities are v_x and v_z. The aerofoil chord is taken as unity, and the ground distance is h.

The basis of any calculation method such as this is to find a distribution of singularities which satisfies the condition that the aerofoil surface $z = z(x)$ is a streamline:

$$\frac{dz}{dx} = \frac{V_{z0} + v_z(x, z)}{V_{x0} + v_x(x, z)}, \tag{1}$$

and then to calculate the total velocity $V(x, z)$ on the surface $z(x)$.

In a completely linearised theory, this process is simplified by assuming

(1) that $v_x(x, z)$ is small compared with V_{x0} and can be ignored in Equation (1);

(2) that $v_z(x, z)$ can be replaced by $v_z(x, 0)$ calculated on the chord line;

(3) that $V(x, z)$ is equal to the total velocity in the x-direction on the chord line, *i.e.*, to $V_{x0} + v_x(x, 0)$.

In dealing with the isolated aerofoil, Weber[13, 14] has introduced some modifications to this procedure which considerably improve the accuracy of the solution. Assumption (1) is retained: this permits the problem to be separated into a 'thickness' problem which is solved by placing a source distribution $q(x)$ along the aerofoil chord line, and a 'lifting' problem solved by a vortex distribution $\gamma(x)$ on the chord line. Assumption (2) is retained in dealing with the thickness problem[13] and also in dealing with the effect of camber[14]; but a better approximation to $v_z(x, z)$ is used to calculate the vortex distribution which represents the circulation due to wing incidence[13]. In place of Assumption (3), it is shown that a better approximation is given by the relation

$$V(x, z) = \frac{V_{x0} + v_x(x, 0)}{\sqrt{\{1 + (dz/dx)^2\}}}. \tag{2}$$

To deal with the problem of the aerofoil near the ground, the same distributions of sources and vortices are used as for the isolated wing, together with their images in the ground plane and an additional vortex distribution. A further simplifying assumption is made, that the singularities can be placed on two lines parallel to the ground plane rather than on the actual chord line and its

image; the velocity increments v_x and v_z are calculated on these lines. This assumption is evidently justifiable as long as the wing incidence α is small, as in practice it must be for attached flow to be maintained.

It should be noted that Assumption (1) is justifiable, for the wing near the ground, only when the lift on the aerofoil is small. For lift coefficients above about 1·0, the circulation round the image aerofoil causes a significant negative velocity $v_x(x, z)$, which cannot be ignored in comparison with V_{x0}. For the case of the simple aerofoil considered here, Assumption (1) can still be made, because the boundary layer around the aerofoil will separate from the surface, so that the whole basic model used in the theory breaks down, at lift coefficients of about 1·0 or less. If, however, an aerofoil with slotted flap or some form of supercirculation is considered, the reduction in stream velocity due to the image circulation can considerably reduce the lift on the aerofoil, as has been shown in simple terms by Young[18]. No consideration of this problem is given here.

The 'thickness' and 'lifting' problems for the simple aerofoil are now considered separately.

2.2. *Wing at Zero Incidence.* A symmetrical aerofoil of semi-thickness $z_t(x)$ is considered, which is at a height h above an infinite ground plane, in a uniform stream V_{x0}. This is represented by a source distribution $q(x)$ on two parallel lines at a distance $2h$ apart, which produces the velocity increments v_{qx} and v_{qz}.

Applying the Assumptions (1) and (2) given in Section 2.1, Equation (1) for this case becomes

$$\frac{dz_t}{dx} = \frac{v_{qz}(x, 0)}{V_{x0}}. \tag{3}$$

It is shown in the Appendix that this leads to the same relation between source strength and aerofoil shape as was obtained by Weber[9] for the isolated case:

$$q(x) = 2V_{x0}(dz_t/dx). \tag{4}$$

It is also shown there that the velocity increments at points on the aerofoil chord line are equal to the velocity increments on the isolated aerofoil plus the additional terms:

$$\frac{\Delta v_{qx}(x, 0)}{V_{x0}} = \frac{1}{\pi}\int_0^1 \frac{dz_t}{dx'}\frac{x - x'}{(x-x')^2 + 4h^2}\,dx' \tag{5}$$

$$\frac{\Delta v_{qz}(x, 0)}{V_{x0}} = \frac{1}{\pi}\int_0^1 \frac{dz_t}{dx'}\frac{2h}{(x-x')^2 + 4h^2}\,dx' \tag{6}$$

which can conveniently be approximated by sum-functions of the aerofoil ordinates at specified points:

$$\frac{\Delta v_{qx}(x_\nu, 0)}{V_{x0}} = S^{(25)}(x_\nu) = \sum_{\mu=1}^{N-1} s_{\mu\nu}{}^{(25)} z_t(x_\mu)$$

$$\frac{\Delta v_{qz}(x_\nu, 0)}{V_{x0}} = S^{(26)}(x_\nu) = \sum_{\mu=1}^{N-1} s_{\mu\nu}{}^{(26)} z_t(x_\mu).$$

The additional vertical velocity given by Equation (6) means that the aerofoil is no longer a streamline of the flow, and can be regarded as an 'induced camber' effect due to the image source distribution. To cancel this velocity, a distribution of vortices along the aerofoil chord line and its image can be added, which induces a vertical velocity equal to $-\Delta v_{qz}$ at all points on the chord line.

The required vortex distribution on two parallel lines can be constructed from a set of standard distributions whose velocity fields have been tabulated by Küchemann and Weber[6]. They have considered the three Birnbaum distributions:

$$\left.\begin{aligned} \gamma_1(x) &= 2\pi V_{x0}\sqrt{\left(\frac{1-x}{x}\right)} \\ \gamma_2(x) &= 2\pi V_{x0}\sqrt{\{1-(1-2x)^2\}} \\ \gamma_3(x) &= 2\pi V_{x0}(1-2x)\sqrt{\{1-(1-2x)^2\}} \end{aligned}\right\} \tag{7}$$

Tables of the non-dimensional velocity increments $v_{xj}^* = v_{xj}/V_{x0}$ and $v_{zj}^* = v_{zj}/V_{x0}$ ($j = 1$ to 3) due to the distributions $\gamma_j(x)$, at points on one of the vortex lines are given in Ref. 6 for various values of the distance $2h$; these values have been plotted in Figs. 1 to 5 of this Report to allow calculations to be made for any value of $h \geqslant \frac{1}{8}$, which is likely to cover all the cases of practical interest.

It should be noted that, in contrast to the definition used in Ref. 6, $\gamma(x)$ is here counted positive when it produces a positive lift force on the aerofoil: *i.e.*, when the local velocities on the upper surface are increased by the presence of the vortex distribution.

It will be observed from the values of v_{zj}^* that the distribution $\gamma_1(x)$, which on the isolated aerofoil produces a constant downwash and thus represents a flat plate at incidence, no longer does so when accompanied by its image distribution. On the other hand $\gamma_2(x)$ still closely represents a circular-arc type of camber-line, though the curvature of the arc represented by a given vortex strength is reduced as the distance between the two lines diminishes.

By using the three distributions (7), the boundary condition can be satisfied at three points, giving three equations of the form

$$c_1 v_{z1} + c_2 v_{z2} + c_3 v_{z3} = -\Delta v_{qz} \tag{8}$$

which can be solved to give the values c_1, c_2 and c_3. The chordwise velocity increment at a point on the chord line is then

$$v_{\gamma x}(x, 0) = c_1 v_{x1} + c_2 v_{x2} + c_3 v_{x3} \pm \tfrac{1}{2}(c_1\gamma_1 + c_2\gamma_2 + c_3\gamma_3). \tag{9}$$

The total velocity increment due to the source and vortex distribution at a point on the chord line is thus

$$\frac{v_x(x, 0)}{V_{x0}} = S^{(1)}(x) + \frac{\Delta v_{qx}}{V_{x0}} + \frac{v_{\gamma x}}{V_{x0}},$$

where $S^{(1)}(x) = \dfrac{1}{\pi}\displaystyle\int_0^1 \frac{dz_t}{dx'}\frac{dx'}{x-x'}$ is the velocity increment on the isolated aerofoil according to Weber's theory[13]. This is conveniently obtained in practice from a sum-function of the aerofoil ordinates at N specified points x_μ, thus: $S^{(1)}(x_\nu) = \displaystyle\sum_{\mu=1}^{N-1} s_{\mu\nu}^{(1)} z_t(x_\mu)$. The coefficients $s_{\mu\nu}^{(1)}$ and the points x_μ, x_ν are tabulated in Ref. 13. In the same paper, a convenient approximate method for calculating the aerofoil slope is also given; this is also obtained as a sum-function of the ordinates at the points x_μ, thus:

$$\frac{dz_t}{dx}(x_\nu) = S^{(2)}(x_\nu) = \sum_{\mu=1}^{N-1} s_{\mu\nu}^{(2)} z_t(x_\mu).$$

Adopting Weber's assumption (Equation (2)), the total velocity at a point on the surface of an aerofoil at zero incidence close to the ground is therefore given by:

$$\frac{V(x)}{V_{x0}} = \frac{1}{\sqrt{\{1+(dz_t/dx)^2\}}}\left\{1 + S^{(1)}(x) + \frac{\Delta v_{qx}}{V_{x0}} + \frac{v_{\gamma x}}{V_{x0}}\right\}$$

$$= \frac{1}{\sqrt{\{1+(S^{(2)}(x))^2\}}}\left\{1 + S^{(1)}(x) + S^{(25)}(x) + \sum_{j=1}^{3} c_j\left(v_{xj}^* \pm \frac{\gamma_j}{2V_{x0}}\right)\right\} \qquad (10)$$

The terms $S^{(1)}(x)$, $S^{(2)}(x)$ and $S^{(25)}(x)$ are conveniently calculated from the appropriate sum-functions given in Ref. 13 and in the Appendix here; the terms v_{xj}^* can be obtained from Figs. 1 and 2. (A minor practical inconvenience arises because the v_{xj}^* are not plotted in Figs. 1 and 2 for the points x_p at which the other terms are obtained, and thus one or other term has to be interpolated, graphically or otherwise.)

The relative importance of the velocity increments due to the image aerofoil can be seen in Fig. 6, which shows the velocity distribution at zero incidence on a 10 per cent thick RAE 101 aerofoil at ground distances $h = 0{\cdot}23$ and $h = 0{\cdot}50$. The term Δv_{qx} is a small increase in velocity on both surfaces of the aerofoil, compared with the velocity on the isolated wing, while the term $v_{\gamma x}$ produces a large increase in lower-surface velocities and a smaller decrease on the upper surface. The net effect is that the upper-surface velocities are changed very little by the proximity of the ground, but the lower-surface velocities are increased. The result is a negative lift force on the aerofoil at zero incidence; the magnitude of this force falls off rapidly with increasing distance h.

Although the discussion in this Section is explicitly concerned with symmetrical aerofoil sections, it is clear that cambered sections could be dealt with equally easily by adding the term (dz_s/dx) to the right-hand side of Equation (8), provided that the camber-line ordinates $z_s(x)$ are sufficiently small to validate the assumption that velocity increments can be calculated on the chord line instead of on the aerofoil surface. Also, the term dz/dx in the factor $\sqrt{\{1+(dz/dx)^2\}}$ introduced in Equation (2) is to be taken as the surface slope, as for the corresponding isolated aerofoil. It is convenient to use Weber's method[14] to calculate $dz_s/dx = S^{(5)}(x)$ as a sum-function of the camber-line ordinates, and replace the first factor in Equation (10) by $1/\sqrt{\{1+(S^{(2)} \pm S^{(5)})^2\}}$ for the cambered aerofoil.

2.3. *Wing at Incidence.* As already pointed out, by making Assumption (1) quoted in Section 2.1, the 'thickness' and 'lift' problems can be separated. For the calculation of the velocities due to thickness on the aerofoil at incidence, the results of Section 2.2 can thus be used; as for the isolated aerofoil, $V_{x0} = V_0 \cos\alpha$.

The velocities due to the circulation round the aerofoil at incidence can be calculated by using a vortex distribution on the chord line and on its image in the ground plane; the calculations are considerably simplified if the vortex distribution on these two oblique lines is replaced by a distribution on two parallel lines, which can be constructed from the three standard distributions $\gamma_j(x)$ given in Equation (7). This simplification is evidently justified if $\tan\alpha$ is small compared with h.

For the isolated thick aerofoil at incidence, Weber[13] has used a vortex distribution on the chord line:

$$\gamma_0(x) = 2V_0 \sin\alpha\left\{1 + \frac{1}{\pi}\int_0^1\left[\frac{dz_t}{dx'} - \frac{2z_t(x')}{1-(1-2x')^2}\right]\frac{dx'}{x-x'}\right\}\sqrt{\left(\frac{1-x}{x}\right)}$$

which can conveniently be written as

$$\gamma_0(x) = 2V_0 \sin\alpha\,(1+S^{(3)}(x))\sqrt{\left(\frac{1-x}{x}\right)} \qquad (11)$$

where the factor $(1+S^{(3)}(x))$ represents the improvement over Assumption (2) of linearised theory referred to in Section 2.1. $S^{(3)}(x)$ can conveniently be calculated by a sum-function of the ordinates in the same way as $S^{(1)}(x)$ and $S^{(2)}(x)$, i.e., as

$$S^{(3)}(x_\nu) = \sum_{\mu=1}^{N-1} s_{\mu\nu}{}^{(3)} z_l(x_\mu)$$

where the coefficients $s_{\mu\nu}{}^{(3)}$ are tabulated in Ref. 13.

It has already been pointed out in Section 2.2 that a vortex distribution proportional to $\sqrt{\left(\frac{1-x}{x}\right)}$ on two parallel lines no longer represents a flat plate at incidence as it does when placed on a single line. For the aerofoil near the ground, therefore, it is necessary to use an additional vortex distribution, which can conveniently be written as

$$\Delta\gamma(x) = d_1\gamma_1(x) + d_2\gamma_2(x) + d_3\gamma_3(x).$$

The vertical velocity components due to $\Delta\gamma(x)$ must compensate for the 'interference' effect of the images of the basic distribution $\gamma_0(x)$. Since these velocity increments are all small compared with that due to the basic distribution, it is assumed that they can be calculated on the chord line instead of the aerofoil surface. Furthermore, since the factor $S^{(3)}$ is proportional to the aerofoil thickness/chord ratio, the term $S^{(3)} \sin\alpha$ is small of second order and can justifiably be ignored in calculating the interference effect of the image. The interference term is then the difference between the vertical velocity increments produced on the chord line by the distribution

$$\gamma(x) = 2V_0 \sin\alpha \sqrt{\left(\frac{1-x}{x}\right)}$$

$$= V_0 \sin\alpha \frac{\gamma_1(x)}{\pi V_{x0}}$$

close to the ground and in isolation, *viz*:

$$\Delta v_z(x) = \frac{V_0 \sin\alpha}{\pi}\{v_{z1}{}^*(x) - (v_{z1}{}^*(x))_{h=\infty}\}$$

where $(v_{z1}{}^*(x))_{h=\infty}$ denotes the value of $v_{z1}(x)/V_{x0}$ as $h \to \infty$, *i.e.*, for the isolated distribution. From the tables in Ref. 6, this has the constant value $-\pi$.

The vertical velocity increment produced by the additional vortex distribution $\Delta\gamma$ must therefore be given by

$$d_1 v_{z1} + d_2 v_{z2} + d_3 v_{z3} = -\Delta v_z(x)$$

$$= -V_0 \sin\alpha \left\{\frac{v_{z1}{}^*}{\pi} + 1\right\},$$

i.e.,

$$\left(\frac{V_0 \sin\alpha}{\pi V_{x0}} + d_1\right) v_{z1} + d_2 v_{z2} + d_3 v_{z3} = -V_0 \sin\alpha. \tag{12}$$

From three such equations, for different values of x, the values of d_1, d_2 and d_3 can be found.

The chordwise velocity increment on the chord line due to the distributions $\gamma_0 + \Delta\gamma$ is therefore

$$\frac{\overline{v_{\gamma x}}}{V_0} = \pm \sin\alpha\,(1+S^{(3)}(x)) \sqrt{\left(\frac{1-x}{x}\right)} + \frac{\sin\alpha}{\pi} v_{x1}{}^* + \sum_{j=1}^{3} d_j v_{xj}{}^* \pm \sum_{j=1}^{3} d_j \frac{\gamma_j}{2V_0}$$

and, using the same assumption, Equation (2), as Weber[13], the total surface velocity including the terms due to aerofoil thickness is:

$$\frac{V(x)}{V_0} = \frac{1}{\sqrt{\{1 + (S^{(2)}(x))^2\}}} \left\{ \left(1 + S^{(1)}(x) + \frac{\Delta v_{q\,x}}{V_0} + \frac{v_{\gamma\,x}}{V_0}\right) \cos\alpha + \frac{\overline{v_{\gamma\,x}}}{V_0} \right\}.$$

It is possible to simplify these calculations somewhat without altering the basic assumptions. In the calculation actually made for the present paper, $\sin\alpha$ in Equation (12) was replaced by $\tan\alpha$ (which is clearly admissible for small values of α), and the boundary condition for a flat plate at incidence near the ground was set up in the form

$$g_1 v_{z\,1} + g_2 v_{z\,2} + g_3 v_{z\,3} = -V_0 \tan\alpha.$$

From three equations of this form, the coefficients g_1, g_2 and g_3 were determined, and the vortex distribution $\gamma_0 + \Delta\gamma$ was taken as

$$(1 + S^{(3)}(x))\, g_1\gamma_1 + g_2\gamma_2 + g_3\gamma_3,$$

where the factor $(1 + S^{(3)}(x))$ was introduced to account for the effect of wing thickness. The chordwise velocity increment was taken as

$$\frac{\overline{v_{\gamma\,x}}}{V_0} = (1 + S^{(3)}(x))\, g_1 \left(v_{x\,1}^* \pm \frac{\gamma_1}{2V_0}\right) + g_2 \left(v_{x\,2}^* \pm \frac{\gamma_2}{2V_0}\right) + g_3 \left(v_{x\,3}^* \pm \frac{\gamma_3}{2V_0}\right)$$

which reduces to the required result for the isolated wing given by Weber[13] as $h \to \infty$, and introduces only a small error in other cases where the use of vortices on two parallel lines is justifiable.

Thus, using Equation (2) again to relate velocities at the aerofoil surface to those on the chord line, the final expression obtained for the velocity at a point on the surface of the aerofoil at incidence becomes

$$\frac{V(x)}{V_0} = \frac{1}{\sqrt{\{1 + (S^{(2)}(x))^2\}}} \left[\left\{ 1 + S^{(1)}(x) + S^{(25)}(x) \pm \sum_{j=1}^{3} \left(c_j v_{x\,j}^* \pm \frac{\gamma_j}{2V_0 \cos\alpha} \right) \right\} \cos\alpha + \right.$$

$$\left. + g_1 (1 + S^{(3)}(x)) \left(v_{x\,1}^* \pm \frac{\gamma_1}{2V_0}\right) + g_2 \left(v_{x\,2}^* \pm \frac{\gamma_2}{2V_0}\right) + g_3 \left(v_{x\,3}^* \pm \frac{\gamma_3}{2V_0}\right) \right]. \qquad (13)$$

At high incidences, the pressure distribution exhibits a large suction peak near the nose on the upper surface, and for practical calculations in this region it is convenient to multiply the numerator and denominator of Equation (13) by $\sqrt{x}$, so that the infinite values of γ_1 and of $S^{(2)}(x)$ at $x = 0$ are avoided. This gives the result:

$$\frac{V(x)}{V_0} = \frac{1}{\sqrt{\{x + \frac{1}{4}(dz/d\sqrt{x})^2\}}} \{P_1(x)\sqrt{x} \pm P_2(x)\sqrt{(1-x)}\} \qquad (14)$$

where

$$P_1(x) = \left(1 + S^{(1)}(x) + S^{(25)}(x) + \sum_{j=1}^{3} c_j v_{x\,j}^*\right) \cos\alpha \pm c_2 \frac{\gamma_2}{2V_0} \pm c_3 \frac{\gamma_3}{2V_0} +$$

$$+ g_1 (1 + S^{(3)}(x)) v_{x\,1}^* + g_2 v_{x\,2}^* + g_3 v_{x\,3}^* \pm g_2 \frac{\gamma_2}{2V_0} \pm g_3 \frac{\gamma_3}{2V_0}$$

and

$$P_2(x) = \pi\{c_1 + g_1(1 + S^{(3)}(x))\}.$$

Equations (13) and (14) have been used to calculate the velocity distributions round a 10 per cent thick RAE 101 aerofoil, at an incidence near the stall, and the results are shown in Fig. 7. The principal effect of the proximity of the ground is a reduction in the velocities on the lower surface, with a slight rearward shift of the stagnation point. The magnitude of the peak velocity is only slightly increased near the ground, but the gradient behind it increases noticeably. The overall lift is increased by the change in lower-surface pressures, and the centre of pressure moves back by about 2 per cent chord.

2.4. *Comparison of the Calculation Method with an Exact Solution for Inviscid Flow.* Although a number of authors[8, 9, 10, 11] have treated the two-dimensional aerofoil near the ground as a problem of potential theory, and applied the method of conformal transformations to obtain exact solutions for inviscid flow, the majority of the solutions have been obtained in the form of infinite series. However, Tomotika, Hasimoto and Urano[10] have obtained solutions in closed form for three special cases of particular aerofoils. Their example A has been used to check the results obtained from the calculation method given in Section 2.

Aerofoil A is illustrated in Fig. 8; it has a thickness/chord ratio of 8·5 per cent with maximum thickness position at about $x/c = 0{\cdot}32$, a cusped trailing-edge, and almost no camber. The aerofoil incidence is 5·17 deg, and the ground distance $h = 0{\cdot}287$. Formulae are given in Ref. 10 which define the detailed shape of the section; an explicit expression for the velocity on the aerofoil surface is not given in Ref. 10, but it was developed by Professor J. C. Cooke for the purpose of this comparison.

Using the calculated section shape, and the other geometrical parameters quoted above, Equations (13) and (14)* have been used to calculate an approximate velocity distribution. In Fig. 9, this is compared with the exact velocity distribution calculated by Cooke, and it can be seen that reasonable agreement has been obtained: the maximum errors in velocity are about 5 per cent, occurring on the rear part of the lower surface.

3. *The Experimental Investigation.* In Sections 2 and 3, no account has been taken of viscosity. Comparisons of the results given by Weber's theory[13] with experiments on isolated two-dimensional aerofoils (particularly that by Brebner and Bagley[12]) have shown that the aerofoil boundary layer has a significant influence on the surface pressure distributions, which must be taken into account if very close agreement is to be obtained between theory and experiment.

As no suitable experimental results were known which could be compared with the theory given in Section 2, a series of experiments were made as part of the present work.

3.1. *Method of Simulating the Ground.* Of the various methods available for performing tests on the effect of ground in a wind-tunnel, the simplest technique is the use of a solid 'ground board' parallel to the tunnel wall. This simple method has two drawbacks: a boundary layer is developed along the surface of the ground board which has no counterpart in the real flow, and which is liable to separate if the aerofoil approaches too close to the ground; and the board divides the wind-tunnel into two channels in which the blockages are generally unequal, so that a circulation is set up around the ground board. The flow past the model is therefore not uniform, and not straight, and it is not possible to say what the 'free-stream' velocity at the model actually is.

* The small camber of the aerofoil was taken into account, in the way suggested in the last paragraph of Section 2.2.

In the present experiment, the boundary layer on the ground board was measured, and a correction to the measured incidence of the aerofoil has been made to allow for its displacement thickness. Also, where separation of the boundary layer on the board was observed, the results have been specifically noted as being probably unreliable. The circulation round the ground board has been prevented, by a method which is believed to be new. A flap on the trailing edge of the ground board was manipulated from outside the tunnel so that the stagnation point was always fixed on the leading edge of the board. To observe movement of the stagnation point, the leading edge was sharpened, and two small pitot tubes were positioned on the surface immediately behind the leading edge; a movement of the stagnation point off the leading edge then provoked a separation on one side or the other, which caused a drop in the pressure recorded by the pitot tube on that side.

3.2. *Details of Model and Apparatus.* The tests were made in the R.A.E. No. 2 $11\frac{1}{2}$ ft $\times$ $8\frac{1}{2}$ ft Wind Tunnel. The model used was a two-dimensional unswept wing, of 10 per cent thick RAE 101 section, which spanned the shorter, vertical, dimension of the tunnel. The model, of 30 in. chord, was equipped with 52 surface orifices for measuring pressures, located around two parallel sections 4 in. apart at the centre of the span. The model was the same as that previously used for the tests reported in Ref. 12; check measurements showed that the section was accurate to within 0·01 in. (*i.e.*, 0·0003c) at the pressure-measuring stations. Transition was not fixed, and the position of transition was not measured in these tests. Pressures were recorded on a bank of multi-tube manometers; the estimated error in pressure coefficients deduced from these measurements is about 0·01. Incidence of the model was measured by a light reflected from a mirror set in the surface of the aerofoil onto a scale on the tunnel window; this gives an accuracy of about 0·01 deg in measuring the nominal incidence.

The ground board was a hollow wooden plate, $11\frac{1}{2}$ ft (*i.e.*, 4·6c) long and 2 in. thick, spanning the vertical dimension of the tunnel, and experiments were made with this plate 7 in., 11 in. and 15 in. from the aerofoil, giving values of $h = 0{\cdot}23$, $0{\cdot}37$ and $0{\cdot}50$. A flap of 10 in. chord (made from $\frac{1}{8}$ in. brass sheet) was hinged at the trailing edge of the ground board, and used as explained in Section 3.1 to adjust the circulation. The sharp leading edge was produced by inserting a brass plate into the rounded leading edge of the wooden board. Three sets of pitot tubes were installed just behind this, at 25·5 in., 51·0 in. and 76·5 in. from the tunnel floor.

The ground board was braced to the tunnel wall on the side remote from the model by six telescopic struts of external diameter $\frac{3}{4}$ in., and the wing itself was braced by two $\frac{3}{8}$ in. diameter steel rods which ran from pivots recessed into the wing, through the ground board and the tunnel wall to a steel joist clamped to the outer structure of the tunnel. The position of the pivots in the model was at 43 per cent chord (dictated by the necessity for avoiding pressure tubes within the model), so the model rotated about this point. It should thus be noted that the nominal ground distances of 7 in., 11 in. and 15 in. refer to the height of the 43 per cent chord position above the ground; as the incidence is varied the height of other stations is altered.

A sketch of the experimental rig is given in Fig. 10.

The boundary layer on the ground was measured at two stations, 59·8 in. and 88·4 in. from the leading edge (*i.e.*, below the leading and trailing edges of the aerofoil), by a rake of six pitot tubes and one static tube, which were connected to a tilting multi-tube manometer. From these measurements, the displacement thickness of the ground boundary layer was calculated, and used to correct the nominal incidence of the aerofoil—*see* Section 3.3.1.

In order to check that the velocity distribution across the tunnel ahead of the model had not been seriously affected by the large wakes of the ground board and its struts, a preliminary test was run with five pitot-static tubes mounted on a boom across the tunnel at the beginning of the working section ahead of the model and ground board (*see* Fig. 10), in one of the standard calibration positions. With the flap on the ground adjusted to give zero circulation around it, the readings of these five tubes showed that the velocity distribution across the tunnel varied by less than $0{\cdot}02\,V_0$, which is similar to the variation in the empty tunnel. This justifies the use of the standard tunnel calibration curves, which relate total head to the measured pressure difference between the settling chamber and working section, in calculating pressure coefficients from the recorded pressures on the wing.

3.3. *Corrections to Experimental Results.* 3.3.1. *Corrections to aerofoil incidence.* The 'nominal incidence' measured by the light and scale system gives the inclination of the part of the wing near the mirror to the axis of the tunnel. This could differ from the true incidence of the sections at which pressure measurements were made, owing to twisting of the model under load, and to an inclination of the flow to the tunnel axis. That the wing twist under load was negligible was checked by temporarily installing a second mirror near the pressure holes, reflecting a second light beam onto the scale. A barely detectable twist, of less than 0·002 deg per 1 deg incidence, was recorded; but as it could not be measured sufficiently accurately, it has been ignored.

The zero of the main light-and-scale system was found by aligning the wing, in the absence of the ground, so that pressures were equal on upper and lower surfaces. When the ground is installed, the influence of the boundary layer on its surface causes a small alteration of flow direction at the model. To allow for this, it was assumed that the stream direction at the model was parallel to the displacement surface of the boundary layer on the ground, and this was assumed to be defined by a straight line drawn through the displacement thicknesses measured below the leading and trailing edges of the aerofoil. Denoting these by δ^*_{LE} and δ^*_{TE}, the increase in incidence of the wing is then

$$\Delta\alpha = \frac{1}{c}(\delta^*_{TE} - \delta^*_{LE}).$$

The values of δ^*_{LE}, δ^*_{TE} and $\Delta\alpha$ found from the measurements are shown in Fig. 11. The results show a smooth variation with incidence, except when the aerofoil has stalled. It will be noted that, above a certain incidence for each ground distance, δ^*_{TE} is smaller than δ^*_{LE}. This may seem surprising at first sight, but it is important to realise that this variation in δ^* does not imply a similar reduction in the boundary-layer thickness itself. As a check on this result, the pressure distribution along the ground board was calculated for $H = 11$ in., $\alpha = 9$ deg, and the development of the boundary layer under this pressure distribution was calculated, using the measured profile at the 'leading-edge' station as initial values. This calculation showed that there was a favourable velocity gradient along the plate, leading to a decreasing momentum thickness and an increasing value of the form parameter H; the average value of $(d\delta^*/dx)$ from the calculation was about $-0{\cdot}004$, compared with $-0{\cdot}006$ from the measurements.

3.3.2. *Corrections to Pressure Measurements.* All the measurements were made at a constant value of the pressure difference $(p_s - p_w)$ between the settling chamber and a station just ahead of the working section. The corresponding flow velocity V_0 in the empty tunnel is then known from the

tunnel calibration, but the actual velocity at the model in this test is higher, due to the large blockage in the tunnel. The blockage corrections to tunnel speed may conveniently be considered in three parts.

The introduction of the ground plate reduced the cross-sectional area of the tunnel along almost the entire length of the working section; since it was adjusted so that no circulation existed around the plate, the change in velocity at the model may be found simply by continuity: the tunnel width is 138 in., and the plate thickness 2 in., so

$$(V_0+\Delta v)136 = V_0 \times 138$$

$$\frac{\Delta v}{V_0} = \frac{2}{136} = 0{\cdot}0147. \tag{15}$$

The solid blockage of the aerofoil itself is found by the standard method of replacing it by an equivalent doublet and calculating the velocity induced at the model position by the images of this doublet in the tunnel walls. For this purpose the effective tunnel is the channel between the ground board and the opposite tunnel wall, and the wing is set off-centre in this tunnel. Batchelor[15] has given the appropriate correction for this case as

$$\frac{\Delta v}{V_0} = \frac{\pi^2}{48}\left(1 + 3\sec^2\frac{\pi a}{h_2}\right)\lambda\left(\frac{t}{h_2}\right)^2 \tag{16}$$

where h_2 is the effective tunnel breadth ($h_2 = 69+H$), H is the distance of the model from the ground, a is the off-centre distance of the model ($a = 34{\cdot}5-\frac{1}{2}H$), (t/c) is the thickness/chord ratio, and λ is Lock's parameter for the aerofoil shape, which in this case is equal to $(4{\cdot}7+47\alpha^2)$.

The correction given by Equation (16) includes the velocity due to the nearest image, in the ground plate, which is a true 'ground effect' and therefore not part of the tunnel correction. The velocity at the model due to this image is

$$\frac{\Delta v}{V_0} = \frac{\lambda t^2}{4(h_2-2a)^2},$$

so the net blockage correction

$$\frac{\Delta v}{V_0} = \lambda\left(\frac{t}{h_2}\right)^2\left[\frac{\pi^2}{48}\left(1 + 3\sec^2\frac{\pi a}{h_2}\right) - \frac{1}{4[1-(2a/h_2)]^2}\right]. \tag{17}$$

The values of this correction $\Delta v/V_0$ are:

α (deg)	$H = 7$ in.	$H = 11$ in.	$H = 15$ in.
0	0·0030	0·0028	0·0025
4	0·0032	0·0029	0·0027
8	0·0036	0·0033	0·0030
10	0·0040	0·0036	0·0033

The induced velocity for a wing in an off-centre position has a small component normal to the wing, but this is negligible because the velocities induced by successive images are of opposite signs, and the largest contribution is a 'ground effect' and thus not accountable as a tunnel correction. The same is true of the normal velocity induced by the images of the vortex which represents the circulation of the wing in Glauert's standard tunnel corrections[16].

The third part of the tunnel correction is that due to the wakes of the model and the other parts of the rig. The wakes may be represented by a distribution of sources, which produce a negative velocity at infinity upstream of the model: to restore the velocity at infinity to the value V_0, a uniform positive velocity Δv must be added to the main flow. For two-dimensional tests, this increment is (*see*, for example, Ref. 16)

$$\frac{\Delta v}{V_0} = \frac{C_D \times c}{4w}$$

where w is the full tunnel width (here $w = 138$ in.), c the chord length and C_D the drag coefficient of the wake-producing body. For the present application, $(C_D \times c)$ is taken as the sum of the appropriate products for three items—the wing, the ground plate and the struts.

For the wing $c = 30$ in., and C_D may be estimated from the results given in Ref. 12 for the wing alone. This gives

α (deg)	C_D	$C_D \times c$
0	0	0
4	0·004	0·120
8	0·012	0·360
10	0·15*	4·50

* This value is appropriate for all 'stalled' cases.

The ground-plate chord is 150 in., and the drag coefficient (assuming that the boundary layer is turbulent from the leading edge and that the disturbance due to the pressure field of the wing is negligible) is 0·00625, so $(C_D \times c) = 0{\cdot}938$.

There are six struts, of diameter $\frac{3}{4}$ in., spanning the gap between the ground plate and the tunnel wall, and two $\frac{3}{8}$ in. diameter struts between the wing and the wall. All these have a drag coefficient of about 1·2 at the wind speeds used in this test. The value of $(C_D \times c)$ would, therefore, be $(6 \times 1{\cdot}2 \times \frac{3}{4}) + (2 \times 1{\cdot}2 \times \frac{3}{8})$, but this assumes the rods span the full width of the tunnel. This value was reduced in proportion to the actual length of the rods, giving

H	$C_D \times c$
7 in.	3·754
11 in.	3·543
15 in.	3·331

The total correction $(\Delta v/V_0)$ for the wakes of the rig is therefore

α (deg)	$H = 7$ in.	$H = 11$ in.	$H = 15$ in.
0	0·0085	0·0081	0·0077
4	0·0087	0·0083	0·0079
8	0·0092	0·0088	0·0084
10 (stall)	0·0167	0·0163	0·0159

The final correction, obtained by adding the values of $\Delta v/V_0$ from Equations (15) and (17) to these wake corrections, is:

α (deg)	$H = 7$ in.	$H = 11$ in.	$H = 15$ in.
0	$\Delta v/V_0 = 0{\cdot}0262$	$0{\cdot}0256$	$0{\cdot}0249$
4	$0{\cdot}0266$	$0{\cdot}0259$	$0{\cdot}0253$
8	$0{\cdot}0275$	$0{\cdot}0268$	$0{\cdot}0261$
10 (stall)	$0{\cdot}0354$	$0{\cdot}0346$	$0{\cdot}0339$

This correction to the main-stream velocity has been employed in calculating all the pressure coefficients presented in Tables 2, 3, 4.

3.4. *Experimental Results.* All the tests were made at a wind speed of 100 ft/sec, giving a Reynolds number based on wing chord of $1{\cdot}6 \times 10^6$. Tests were made for a range of nominal incidences from zero to 10 deg, for ground distances of 7 in., 11 in. and 15 in. (i.e., $h = 0{\cdot}23$, $0{\cdot}37$ and $0{\cdot}50$). The results obtained at $h = 0{\cdot}23$ above 4 deg incidence are likely to be unreliable because the boundary layer along the ground board appeared to have separated.

The pressure coefficients calculated from the measured pressures are presented in Tables 2, 3 and 4; they have been integrated to give normal-force, tangential-force, lift, drag and pitching moment coefficients which are tabulated in Table 5. A selection of the experimental pressure distributions is shown in Figs. 12, 13 and 15, and the lift and pitching-moment coefficients are presented in Fig. 14. Comparison between these results and the theoretical results of Section 2 is made below, in Section 4, but certain features of the results in Fig. 14 will be noted. At small incidences the lift decreases, and even becomes negative, as the wing approaches the ground, but at higher incidences the lift increases steadily as the wing nears the ground. This behaviour reflects firstly the negative 'induced camber' effect of the image at zero incidence, and secondly the increase in lift slope due primarily to the increased pressures on the lower surface at incidence.

3.5. *Ground effect on* $C_{L\max}$. At high incidences, it appeared that two possible flows could be established on the wing. Normally, by increasing incidence steadily at a fixed tunnel speed, $C_{L\max}$ was reached when the short bubble near the leading edge burst and gave place to a long bubble covering most of the aerofoil chord.* However, there was a marked hysteresis effect, for the long bubble persisted as incidence was reduced, down to an incidence well below that at which it first appeared. No accurate value of $C_{L\max}$ for the 'short bubble' flow could be defined, because this flow was not stable and tended to collapse spontaneously to the 'long bubble' flow after a short period of time. The two branches of the C_L curve are shown in Fig. 14: full pressure measurements were not available in the hysteresis region, where the upper branch is an extrapolation of the earlier part of the curve up to the highest incidence at which the short bubble flow persisted long enough for a measurement to be obtained (*i.e.*, about 5 seconds).

This hysteresis in the $C_L - \alpha$ curves is not purely a 'ground effect': it was also observed (though not recorded) in the tests without ground on the same aerofoil[12]. However, it was definitely more pronounced in the present tests, presumably because the changes in pressure distribution due to the ground have brought the aerofoil closer to the boundary between short bubble and long bubble

* *See* Ref. 1 for a detailed explanation of the mechanism of this process.

stalling types[1]. This tends to show that the influence of the ground on certain aerofoils might in fact change their stalling behaviour considerably, as was suggested in the Introduction. However, this sort of change must depend on the Reynolds number of the flow (*see* Ref. 1); this seems to preclude any possibility of finding a simple method for predicting the variation of $C_{L\max}$ with ground height for this type of section.

The values of $C_{L\max}$ obtained on the lower branches of the lift curves do not vary significantly with ground distance, though they are all considerably smaller than the value obtained on the upper branch of the curve for the isolated wing[12]. Owing to the increase in lift slope as the wing approaches the ground, there is a significant reduction in the incidence at which $C_{L\max}$ is reached with diminishing ground distance.

4. *Comparison between Theory and Experiment.* Experimental pressure distributions at near-zero incidence are given in Fig. 12 for $h = 0{\cdot}23$, $0{\cdot}37$ and $0{\cdot}50$, compared with the corresponding theoretical distributions calculated by the method of Section 2 (taking $C_p = 1 - (V/V_0)^2$). The incidence terms in the pressure distribution are very small so that these results are essentially a check on Equation (10).

The agreement between theory and experiment seems generally satisfactory, although there are small differences at various points: the most noteworthy probably being near the nose where the experimental results on the upper and lower surface cross over further back than the theoretical results. The most probable explanation of these discrepancies lies in the correction made for the boundary layer along the ground plate: the assumption that the displacement surface can be adequately defined by a straight line between the two measured values of δ^* is rather crude, and it seems likely that this surface is curved which would introduce another small 'camber' of the flow past the aerofoil.

The experimental pressure distribution for $h = 0{\cdot}37$, $\alpha = 8{\cdot}63$ deg is compared in Fig. 15 with that calculated from Equation (13). This shows good agreement in general, except that the experimental pressures and suctions are almost everywhere smaller in magnitude than the theoretical, and there is a divergence between theory and experiment near the trailing edge. It seems likely that the differences are due to the effect of the boundary layer on the aerofoil, and this is confirmed by the comparison given in Fig. 16.

In Fig. 16, theoretical pressures calculated from Equation (13) are shown for three values of h, corresponding to the distances from the ground of the leading edge, trailing edge and the 43 per cent chord pivot point—the latter being the 'nominal' ground distance used in the rest of this Report. In each case, the theoretical results have been corrected to allow for the influence of the boundary layer, and the magnitude of this correction is indicated on the figure.

The boundary layer on the aerofoil was not measured in the present tests, and it is not yet a practical proposition to calculate the boundary-layer development entirely by theoretical methods. The correction for the aerofoil boundary layer in Fig. 16 was therefore taken from the results of Ref. 12, where the boundary layer on the wing was measured in the absence of ground. Calculations were made in Ref. 12 of the inviscid pressure distribution, and of the pressure distribution on the wing with the measured boundary layer. The difference between thse two calculated distributions† for the wing without ground has been applied to each of the three calculated distributions to obtain

† The calculations made in Ref. 12 were actually for $\alpha = 4{\cdot}09$ deg and $\alpha = 8{\cdot}18$ deg, so the results used here for $\alpha = 8{\cdot}63$ deg were obtained by extrapolation.

the result given in Fig. 16. Since the change in pressure distribution due to the presence of the ground is small, the change in boundary-layer development should be small, and it should be within the limits of experimental error to use the correction from the isolated wing also when the wing is near the ground.

The comparison in Fig. 16 between the theoretical results obtained using three different values for h suggests that the 'nominal' distance gives a better agreement with the experimental results than either of the others. In general, the height of the mid-chord point would be equally satisfactory, and would be a more convenient choice than the 43 per cent chord point used here.

The fact that different results are obtained for the three different values of h indicates that the assumption, made in Section 2.3, that the aerofoil and its image could be adequately represented by a vortex distribution on two parallel lines, is not strictly valid for this case: here $h = 0{\cdot}37$ and $\tan \alpha = 0{\cdot}1518$ so the condition $h \gg \tan \alpha$ is clearly violated.

5. *Conclusions.* The method of calculating the pressure distribution on a two-dimensional wing near the ground which is developed here is based essentially on Tani's method[5], but an extended source distribution is used to represent the aerofoil and its image instead of the two doublets used by Tani. A distribution of vortices on two parallel lines is used to represent the aerofoil at incidence and its image; the velocity field due to such a distribution has been tabulated by Küchemann and Weber[6], and is also presented in Figs. 1 to 5 of the present paper. Comparison with a series of experimental measurements on a 10 per cent thick RAE 101 aerofoil at distances between $0{\cdot}5$ chord and $0{\cdot}23$ chord from the ground shows that good agreement is obtained, provided allowance is made for the boundary layers on the aerofoil and on the ground board. These comparisons suggest that the appropriate distance to use when calculating the pressure on an aerofoil at incidence above the ground is the height of the mid-chord point.

The investigation was originally undertaken to find out whether the influence of the ground could be sufficient to cause a marked change in $C_{L\max}$ as the wing approached the ground, due to a change in stalling behaviour caused by a change in the development of the laminar-separation bubble near the leading edge. The evidence obtained suggests that this might indeed be the case in some circumstances, although in the present instance the only effect of proximity to the ground was to make more obvious a hysteresis loop in the lift curve at high incidence which was already present without the ground. The actual variation of $C_{L\max}$ with ground height was small, although the increase in lift slope as the wing approached the ground caused a significant reduction in the incidence at which $C_{L\max}$ was reached.

LIST OF PRINCIPAL SYMBOLS

C_D, C_L, C_M, C_N, C_p, C_T — Coefficients of drag, lift, pitching moment, normal force, pressure and tangential force

$C_{L\max}$ — Maximum lift coefficient

h — Height of aerofoil (mid-chord point in theories; 43 per cent chord point in experiments; unless otherwise stated) above ground. Aerofoil chord used as unit distance

H — Height of aerofoil above ground in inches

$q(x)$ — Source distribution used to represent aerofoil thickness

$$S^{(1)}(x_\nu) = \sum_{\mu=1}^{N-1} s_{\mu\nu}^{(1)} z_t(x_\mu) = \frac{1}{\pi}\int_0^1 \frac{dz_t}{dx'}\frac{dx'}{x_\nu - x'}$$

$$S^{(2)}(x_\nu) = \sum_{\mu=1}^{N-1} s_{\mu\nu}^{(2)} z_t(x_\mu) = \frac{dz_t}{dx}(x_\nu)$$

$$S^{(3)}(x_\nu) = \sum_{\mu=1}^{N-1} s_{\mu\nu}^{(3)} z_t(x_\mu) = \frac{1}{\pi}\int_0^1 \left[\frac{dz_t}{dx'} - \frac{2z_t(x')}{1-(1-2x')^2}\right]\frac{dx'}{x_\nu - x'}$$

$$S^{(5)}(x_\nu) = \sum_{\mu=1}^{N-1} s_{\mu\nu}^{(5)} z_s(x_\mu) = \frac{dz_s}{dx}(x_\nu)$$

} *See* Refs. 13 and 14

$$S^{(25)}(x_\nu) = \sum_{\mu=1}^{N-1} s_{\mu\nu}^{(25)} z_t(x_\mu) = \Delta v_{qx}(x_\nu)$$

$$S^{(26)}(x_\nu) = \sum_{\mu=1}^{N-1} s_{\mu\nu}^{(26)} z_t(x_\mu) = \Delta v_{qz}(x_\nu)$$

} *See* Appendix

$V(x, z)$ — Total velocity at point (x, z)

V_0 — Free-stream velocity

V_{x0}, V_{z0} — Components of V_0 in x and z directions

v_x, v_z — Velocity increments in x and z directions

v_{qx}, v_{qz} — Velocity increments due to source distribution

Δv_{qx}, Δv_{qz} — Velocity increments due to image sources—*see* Equations (5) and (6)

v_{xj}, v_{zj} — Velocity increments due to vortex distributions γ_j

v_{xj}^*, v_{zj}^* = v_{xj}/V_{x0}, v_{zj}/V_{x0}

x, z — Cartesian co-ordinates, x along wing chordline, z perpendicular upwards

$z_t(x)$ — Aerofoil thickness ordinate

$z_s(x)$ — Aerofoil camber-line ordinate

(83081)

LIST OF PRINCIPAL SYMBOLS—*continued*

α	Aerofoil incidence
α_{NOM}	Nominal incidence in tunnel
$\Delta\alpha$	Correction for effect of boundary layer on ground plate
δ^*	Displacement thickness of boundary layer on ground plate
$\gamma(x)$	Vortex distribution used to represent circulation round aerofoil
$\gamma_0(x)$	Vortex distribution used for isolated aerofoil—*see* Equation (11)
$\gamma_1, \gamma_2, \gamma_3, \gamma_j$	Standard vortex distributions defined in Equation (7)

REFERENCES

No.	*Author*	*Title, etc.*
1	L. F. Crabtree	The formation of regions of separated flow on wing surfaces. Part 2.—Laminar separation bubbles and the mechanism of the leading-edge stall. A.R.C. R. & M. 3122. July, 1957.
2	P. de Haller	La portance et la trainée induite minimum d'une aile au voisinage du sol. Mitt. a.d. Inst. f. Aerodynamik d. Tech. Hochschule Zurich. No. 5. 1936.
3	M. N. Wood and W. J. G. Trebble	Low speed tunnel measurements of the ground effect on a 1/5th scale model of the *Swift*. A.R.C. C.P. 458. May, 1957.
4	R. M. Licher	Increase in lift for two- and three-dimensional wings near the ground. Douglas Aircraft Co., Santa Monica Division. Report SM-22615. October, 1956.
5	I. Tani	On the effect of the ground upon the lift of a monoplane wing. *Journal of the A.R.I.*, Tokyo Imperial University. No. 96. p. 684. 1932. (This paper is in Japanese; an English version with later additions is: I. Tani, M. Taima and S. Simidu—A.R.I., Tokyo Imperial University. Report 156. 1937.)

REFERENCES—*continued*

No.	*Author*	*Title, etc.*
6	D. Küchemann and J. Weber ..	*Aerodynamics of propulsion.* McGraw-Hill, New York, 1953.
7	S. Tomotika and others	The lift on a flat plate placed near a plane wall. A.R.I., Tokyo Imperial University, Report 97 (1933); extended in Report 120 (1935); Report 152 (1937); Report 182 (1939).
8	T. H. Havelock	The lift and moment on a flat plate in a stream of finite width. *Proc. Roy. Soc. A.* Vol. 166. p. 178. 1938.
9	A. E. Green	The two-dimensional aerofoil in a bounded stream. *Quart. J. Math.* Vol. 18. p. 167. 1947.
10	S. Tomotika, Z. Hasimoto and K. Urano	The forces acting on an aerofoil of approximate Joukowski type in a stream bounded by a plane wall. *Quart. J. Mech. App. Math.* Vol. 4. p. 289. 1951.
11	H. Fujikawa	The lift on the symmetrical Joukowski aerofoil in a stream bounded by a plane wall. *J. Phys. Soc. Japan.* Vol. 9. p. 233. 1954.
12	G. G. Brebner and J. A. Bagley ..	Pressure and boundary-layer measurements on a two-dimensional wing at low speed. A.R.C. R. & M. 2886. February, 1952.
13	J. Weber	The calculation of the pressure distribution over the surface of two-dimensional and swept wings with symmetrical aerofoil sections. A.R.C. R. & M. 2918. July, 1953.
14	J. Weber	The calculation of the pressure distribution on the surface of thick cambered wings and the design of wings with given pressure distribution. A.R.C. R. & M. 3026. June, 1955.
15	G. K. Batchelor	Interference on wings, bodies and airscrews in a closed tunnel of octagonal section. Australian Council for Aeronautics Report ACA.5. March, 1944.
16	R. C. Pankhurst and D. W. Holder	*Wind tunnel technique.* Chapter 8. Pitman, London. 1952.
17	J. Weber	The calculation of the pressure distribution on thick wings of small aspect ratio at zero lift in subsonic flow. A.R.C. R. & M. 2993. September, 1954.
18	A. D. Young	A note on ground effect on the lift due to a jet flap. A.R.C. 19,971. March, 1958.

APPENDIX

The Velocity Field of a Source Distribution on Two Parallel Lines

Sources of strength $q(x)$ are distributed along two parallel lines $z = \pm h$, between the points $x = 0$ and $x = 1$. The velocity increments induced by these distributions at any point (x, z) are then:

$$v_x(x, z) = \int_0^1 \frac{q(x')}{2\pi} \left\{ \frac{(x-x')}{(x-x')^2 + (z-h)^2} + \frac{(x-x')}{(x-x')^2 + (z+h)^2} \right\} dx' \tag{18}$$

$$v_z(x, z) = \int_0^1 \frac{q(x')}{2\pi} \left\{ \frac{(z-h)}{(x-x')^2 + (z-h)^2} + \frac{(z+h)}{(x-x')^2 + (z+h)^2} \right\} dx' . \tag{19}$$

These integrands have singularities at the point $x = x'$ on the lines $z = \pm h$. They may be evaluated by considering the limits as $|z| \to h$, treating separately the integration over a small region of width 2ϵ across the singularity. Within this region, average values of the non-singular terms can be taken.

Treating Equation (19) thus,

$$v_z(x, h) = \operatorname*{Lim}_{\epsilon \to 0} \int_0^{x-\epsilon} + \int_{x+\epsilon}^1 \left(\frac{q(x')}{2\pi} \cdot \frac{2h}{(x-x')^2 + 4h^2} \right) dx' + \\ + \operatorname*{Lim}_{\substack{\epsilon \to 0 \\ z \to h}} \int_{x-\epsilon}^{x+\epsilon} \frac{q(x)}{2\pi} \left\{ \frac{z-h}{(x-x')^2 + (z-h)^2} + \frac{2h}{4h^2} \right\} dx' \tag{20}$$

Setting $x - x' = y$, the second integral in Equation (20) can be written:

$$\frac{q(x)}{2\pi} \left\{ \operatorname*{Lim}_{\substack{\epsilon \to 0 \\ z \to h}} \int_{-\epsilon}^{+\epsilon} \frac{(z-h)}{y^2 + (z-h)^2} dy + \frac{1}{2h} \operatorname*{Lim}_{\epsilon \to 0} \int_{-\epsilon}^{+\epsilon} dy \right\} \\ = \frac{q(x)}{2\pi} 2 \operatorname*{Lim}_{\substack{\epsilon \to 0 \\ z \to h}} \left\{ \tan^{-1} \left(\frac{\epsilon}{z-h} \right) \right\} = \pm \frac{q(x)}{2}$$

taking the limit $z \to h$ first.

Thus the vertical velocity increment is

$$v_z(x, h) = \int_0^1 \frac{q(x')}{2\pi} \frac{2h}{(x-x')^2 - 4h^2} dx' \pm \frac{q(x)}{2} . \tag{21}$$

The discontinuity in vertical velocity as the source distribution is crossed is the same as occurs for the single line of sources used by Weber[13] to represent the isolated aerofoil. Thus the relation between the source strength and the aerofoil thickness distribution $z_t(x)$ is

$$q(x) = 2V_{x0}(dz_t/dx),$$

for the aerofoil near the ground just as for the isolated aerofoil, using the boundary condition (Equation (1)) with the Assumptions (1) and (2) of linearised theory listed in Section 2.1.

Applying the same integration technique to Equation (18) shows that

$$v_x(x, h) = \int_0^1 \frac{q(x')}{2\pi} \frac{x - x'}{(x-x')^2 + 4h^2} dx' + \int_0^1 \frac{q(x')}{2\pi} \frac{dx'}{x - x'} . \tag{22}$$

The second term here is the velocity increment due to a single line of sources. The first terms in (21) and (22) thus represent the 'ground effect' due to the line of image sources. They can be written as

$$\left.\begin{aligned}\frac{\Delta v_{q\,x}(x)}{V_{x\,0}} &= \frac{1}{\pi}\int_0^1 \frac{dz_l}{dx'}\frac{x-x'}{(x-x')^2+4h^2}\,dx' \\ \frac{\Delta v_{q\,z}(x)}{V_{x\,0}} &= \frac{1}{\pi}\int_0^1 \frac{dz_l}{dx'}\frac{2h}{(x-x')^2+4h^2}\,dx'\end{aligned}\right\} \tag{23}$$

Both these integrals are of the form $I(x) = \frac{1}{\pi}\int_0^1 \frac{dz}{dx'}\,g(x')\,dx'$; Weber has shown in the Appendix of Ref. 17 how such an integral can be approximated by a sum-function of the aerofoil section ordinates at N specified points x_μ. At any one point x_ν of this set:

$$I(x_\nu) = \sum_{\mu=1}^{N-1} s_{\mu\nu}^{(1)}(x_\mu - x_\nu)^2 \left(\frac{dg}{dx'}\right)_{x'=x_\mu} z_l(x_\mu)$$

where the coefficients $s_{\mu\nu}^{(1)}$ are defined and tabulated in Ref. 9, together with the N points x_μ. This procedure is valid, provided that $(x-x')\,g(x')$ and $\frac{d}{dx'}\{(x-x')\,g(x')\}$ are finite and continuous for $0 \leqslant x' \leqslant 1$.

Approximate values for the axial and transverse velocity increments can thus be obtained by applying this technique to Equations (23); the results are

$$\frac{\Delta v_{q\,x}(x_\nu)}{V_{x\,0}} = \sum_{\mu=1}^{N-1} s_{\mu\nu}^{(25)} z_l(x_\mu)$$

and

$$\frac{\Delta v_{q\,z}(x_\nu)}{V_{x\,0}} = \sum_{\mu=1}^{N-1} s_{\mu\nu}^{(26)} z_l(x_\mu),$$

where

$$s_{\mu\nu}^{(25)} = s_{\mu\nu}^{(1)}\frac{(x_\nu-x_\mu)^2-4h^2}{\{(x_\nu-x_\mu)^2+4h^2\}^2}(x_\nu-x_\mu)^2$$

and

$$s_{\mu\nu}^{(26)} = s_{\mu\nu}^{(1)}\frac{4h(x_\nu-x_\mu)^3}{\{(x_\nu-x_\mu)^2+4h^2\}^2}. \tag{24}$$

These velocity increments are small, and it will normally be sufficient in practice to take $N = 8$ in Equations (24), which permits the evaluation of $\Delta v_{q\,x}$ and $\Delta v_{q\,z}$ at seven chordwise stations. Values of the coefficients $s_{\mu\nu}^{(25)}$ and $s_{\mu\nu}^{(26)}$ for $h = \frac{1}{2}$ and $h = 1$ are tabulated in Table 1.

TABLE 1

The Coefficients $s_{\mu\nu}^{(25)}$ and $s_{\mu\nu}^{(26)}$, for $N = 8$, $h = \frac{1}{2}$

$s_{\mu\nu}^{(25)}$

x_μ	μ	$\nu = 1$	$\nu = 2$	$\nu = 3$	$\nu = 4$	$\nu = 5$	$\nu = 6$	$\nu = 7$
0·9619	1	0	0·046	0	0·026	0	0·006	0
0·8536	2	0·085	0	0·082	0	0·037	0	0·011
0·6913	3	0	0·107	0	0·104	0	0·048	0
0·5000	4	0·067	0	0·112	0	0·112	0	0·067
0·3087	5	0	0·048	0	0·104	0	0·107	0
0·1464	6	0·011	0	0·037	0	0·082	0	0·085
0·0381	7	0	0·006	0	0·026	0	0·046	0

$s_{\mu\nu}^{(26)}$

x_μ	μ	$\nu = 1$	$\nu = 2$	$\nu = 3$	$\nu = 4$	$\nu = 5$	$\nu = 6$	$\nu = 7$
0·9619	1	0	+0·010	0	+0·030	0	+0·028	0
0·8536	2	−0·019	0	+0·027	0	+0·057	0	+0·052
0·6913	3	0	−0·036	0	+0·041	0	+0·074	0
0·5000	4	−0·078	0	−0·044	0	+0·044	0	+0·078
0·3087	5	0	−0·075	0	−0·041	0	+0·036	0
0·1464	6	−0·052	0	−0·057	0	−0·027	0	+0·019
0·0381	7	0	−0·028	0	−0·030	0	−0·010	0

The Coefficients $s_{\mu\nu}^{(25)}$ and $s_{\mu\nu}^{(26)}$, for $N = 8$, $h = 1$

$s_{\mu\nu}^{(25)}$

x_μ	μ	$\nu = 1$	$\nu = 2$	$\nu = 3$	$\nu = 4$	$\nu = 5$	$\nu = 6$	$\nu = 7$
0·9619	1	0	0·012	0	0·010	0	0·007	0
0·8536	2	0·022	0	0·022	0	0·018	0	0·014
0·6913	3	0	0·028	0	0·028	0	0·023	0
0·5000	4	0·027	0	0·030	0	0·030	0	0·027
0·3087	5	0	0·023	0	0·028	0	0·028	0
0·1464	6	0·014	0	0·018	0	0·022	0	0·022
0·0381	7	0	0·007	0	0·010	0	0·012	0

$s_{\mu\nu}^{(26)}$

x_μ	μ	$\nu = 1$	$\nu = 2$	$\nu = 3$	$\nu = 4$	$\nu = 5$	$\nu = 6$	$\nu = 7$
0·9619	1	0	+0·001	0	+0·005	0	+0·007	0
0·8536	2	−0·002	0	+0·004	0	+0·010	0	+0·013
0·6913	3	0	−0·005	0	+0·005	0	+0·014	0
0·5000	4	−0·013	0	−0·006	0	+0·006	0	+0·013
0·3087	5	0	−0·014	0	−0·005	0	+0·005	0
0·1464	6	−0·013	0	−0·010	0	−0·004	0	+0·002
0·0381	7	0	−0·007	0	−0·005	0	−0·001	0

TABLE 2

Measured Pressure Coefficients. Ground distance 7 in. ($h = 0{\cdot}23$)

Upper surface

x	$\alpha = 0{\cdot}25°$	$\alpha = 3{\cdot}81°$	$\alpha = 5{\cdot}43°$ *	$\alpha = 6{\cdot}69°$ *	$\alpha = 6{\cdot}93°$ *	$\alpha = 9{\cdot}21°$ *
0	1·00	−0·61	−2·39	−4·56	−1·85	−0·54
0·005	+0·05	−1·96	−3·23	−4·96	−1·90	−0·56
0·007	−0·04	−1·95	−3·15	−4·88	−1·91	−0·57
0·011	−0·16	−1·65	−2·98	−3·27	−1·88	−0·57
0·024	−0·25	−1·39	−1·70	−2·44	−1·90	−0·56
0·047	−0·32	−0·96	−1·43	−1·86	−1·94	−0·56
0·073	−0·34	−0·87	−1·21	−1·52	−1·84	−0·53
0·098	−0·36	−0·79	−1·07	−1·33	−1·74	−0·57
0·148	−0·35	−0·67	−0·88	−1·07	−1·36	−0·55
0·198	−0·36	−0·61	−0·76	−0·92	−0·96	−0·57
0·297	−0·36	−0·54	−0·62	−0·71	−0·60	−0·59
0·348	−0·33	−0·47	−0·53	−0·61	−0·48	−0·62
0·396	−0·30	−0·41	−0·46	−0·52	−0·41	−0·61
0·447	−0·27	−0·35	−0·39	−0·43	−0·35	−0·62
0·497	−0·23	−0·29	−0·31	−0·35	−0·29	−0·62
0·548	−0·17	−0·25	−0·26	−0·28	−0·24	−0·62
0·596	−0·14	−0·20	−0·21	−0·23	−0·19	−0·61
0·647	−0·12	−0·16	−0·16	−0·17	−0·15	−0·62
0·696	−0·09	−0·11	−0·11	−0·11	−0·10	−0·60
0·748	−0·06	−0·07	−0·06	−0·06	−0·07	−0·60
0·795	−0·03	−0·03	−0·01	−0·01	−0·03	−0·58
0·848	0	+0·02	+0·04	+0·02	0	−0·56
0·896	+0·02	0·06	0·07	0·09	+0·03	−0·54
0·948	0·06	0·11	0·14	0·14	0·05	−0·49
0·967	0·08	0·13	0·14	0·15	0·05	−0·46
1·000	0·13	0·18	0·19	0·19	0·09	−0·41

* For $\alpha > 4°$ the boundary layer on the ground appeared to have separated, and these results are therefore unreliable.

TABLE 2—*continued*

Lower surface

x	$\alpha = 0{\cdot}25°$	$\alpha = 3{\cdot}81°$	$\alpha = 5{\cdot}43°$ *	$\alpha = 6{\cdot}69°$ *	$\alpha = 6{\cdot}93°$ *	$\alpha = 9{\cdot}21°$ *
0·006	0·33	0·99	0·81	0·36	0·73	0·90
0·007	0·17	0·99	0·91	0·62	0·86	0·95
0·014	+0·07	0·95	1·00	0·89	0·97	0·99
0·026	−0·11	0·76	0·95	1·00	0·99	—
0·050	−0·24	0·55	0·78	0·90	0·86	0·82
0·075	−0·32	0·42	0·67	0·80	0·76	0·74
0·100	−0·37	0·34	0·58	0·72	0·68	0·66
0·149	−0·42	0·25	0·48	0·61	0·59	0·56
0·200	−0·46	0·18	0·41	0·54	0·52	0·50
0·298	−0·53	0·08	0·32	0·46	0·43	0·38
0·348	−0·50	0·06	0·29	0·43	0·40	0·35
0·398	−0·47	0·06	0·28	0·42	0·38	0·32
0·448	−0·43	0·05	0·26	0·40	0·36	0·27
0·498	−0·38	0·05	0·25	0·38	0·35	0·25
0·548	−0·33	0·06	0·25	0·38	0·33	0·21
0·599	−0·27	0·08	0·25	0·36	0·31	0·16
0·647	−0·21	0·08	0·24	0·35	0·29	0·12
0·698	−0·16	0·10	0·24	0·34	0·28	0·09
0·747	−0·10	0·11	0·24	0·33	0·27	+0·04
0·797	−0·07	0·12	0·23	0·30	0·25	−0·01
0·848	−0·02	0·14	0·23	0·29	0·23	−0·07
0·897	+0·01	0·14	0·22	0·27	0·21	−0·13
0·948	0·05	0·14	0·21	0·23	0·16	−0·23
0·967	0·08	0·15	0·21	0·22	0·15	−0·27

* For $\alpha > 4°$ the boundary layer on the ground appeared to have separated, and these results are therefore unreliable.

TABLE 3

Measured Pressure Coefficients. Ground distance 11 *in.* ($h = 0{\cdot}37$)

Upper surface

x	$\alpha = 0{\cdot}20°$	$\alpha = 4{\cdot}02°$	$\alpha = 5{\cdot}87°$	$\alpha = 6{\cdot}79°$	$\alpha = 7{\cdot}71°$	$\alpha = 8{\cdot}17°$	$\alpha = 8{\cdot}63°$	$\alpha = 9{\cdot}10°$
0	0·99	−1·23	−2·21	−3·19	−4·31	−4·84	−5·42	−0·89
0·005	0·06	−1·97	−3·16	−3·84	−4·76	−5·25	−5·72	−0·82
0·007	+0·03	−1·97	−3·07	−3·74	−4·67	−5·19	−5·67	−1·02
0·011	−0·14	−1·67	−2·84	−3·61	−3·39	−3·34	−3·47	−1·02
0·024	−0·26	−1·41	−1·65	−2·03	−2·40	−2·57	−2·71	−1·02
0·047	−0·33	−1·05	−1·43	−1·62	−1·84	−1·94	−2·01	−1·02
0·073	−0·35	−0·91	−1·20	−1·35	−1·51	−1·57	−1·64	−1·02
0·098	−0·35	−0·82	−1·05	−1·15	−1·31	−1·36	−1·41	−1·02
0·148	−0·35	−0·70	−0·85	−0·94	−1·05	−1·09	−1·12	−1·02
0·198	−0·36	−0·65	−0·77	−0·84	−0·92	−0·96	−0·96	−1·02
0·297	−0·34	−0·54	−0·63	−0·69	−0·73	−0·70	−0·77	−0·83
0·348	−0·31	−0·48	−0·55	−0·66	−0·62	−0·59	−0·66	−0·80
0·396	−0·29	−0·42	−0·48	−0·51	−0·53	−0·51	−0·56	−0·76
0·447	−0·25	−0·35	−0·40	−0·43	−0·45	−0·43	−0·47	−0·69
0·497	−0·22	−0·29	−0·33	−0·35	−0·37	−0·34	−0·38	−0·66
0·548	−0·15	−0·24	−0·27	−0·29	−0·30	−0·28	−0·31	−0·62
0·596	−0·12	−0·21	−0·25	−0·24	−0·24	−0·22	−0·25	−0·54
0·647	−0·11	−0·17	−0·17	−0·18	−0·19	−0·17	−0·19	−0·48
0·696	−0·07	−0·12	−0·12	−0·13	−0·13	−0·11	−0·13	−0·48
0·748	−0·04	−0·07	−0·07	−0·08	−0·07	−0·05	−0·08	−0·41
0·795	−0·02	−0·04	−0·03	−0·03	−0·02	−0·01	−0·04	−0·37
0·848	0	0	+0·01	+0·01	+0·02	+0·04	+0·02	−0·37
0·896	+0·02	+0·03	0·06	0·06	0·07	0·08	0·07	−0·34
0·948	0·07	0·09	0·12	0·11	0·12	0·13	0·11	−0·27
0·967	0·09	0·12	0·14	0·13	0·14	0·14	0·12	−0·25
1·000	0·14	0·16	0·17	0·17	0·17	0·16	0·15	−0·22

TABLE 3—*continued*

Lower surface

x	$\alpha = 0{\cdot}20°$	$\alpha = 4{\cdot}02°$	$\alpha = 5{\cdot}87°$	$\alpha = 6{\cdot}79°$	$\alpha = 7{\cdot}71°$	$\alpha = 8{\cdot}17°$	$\alpha = 8{\cdot}63°$	$\alpha = 9{\cdot}10°$
0·006	0·34	1·00	0·84	0·66	0·41	0·29	0·14	0·85
0·007	0·18	1·00	0·94	0·82	0·66	0·55	0·45	0·91
0·014	+0·08	·0·94	1·00	0·97	0·90	0·86	0·80	0·98
0·026	−0·08	0·72	0·93	0·98	1·00	0·97	1·00	0·95
0·050	−0·18	0·54	0·73	0·81	0·87	0·87	0·93	0·80
0·075	−0·25	0·37	0·61	0·69	0·77	0·77	0·82	0·69
0·100	−0·28	0·30	0·52	0·61	0·68	0·69	0·74	0·53
0·149	−0·31	0·21	0·41	0·49	0·56	0·58	0·62	0·50
0·200	−0·34	0·14	0·33	0·40	0·48	0·50	0·54	0·33
0·298	−0·36	0·05	0·23	0·30	0·37	0·40	0·43	0·31
0·348	−0·34	0·04	0·22	0·28	0·35	0·37	0·40	0·27
0·398	−0·31	0·04	0·21	0·26	0·33	0·35	0·37	0·24
0·448	−0·29	0·04	0·20	0·25	0·31	0·34	0·36	0·22
0·498	−0·25	0·05	0·19	0·25	0·30	0·33	0·35	0·20
0·548	−0·21	0·06	0·19	0·24	0·29	0·31	0·33	0·18
0·599	−0·16	0·07	0·19	0·23	0·28	0·30	0·32	0·17
0·647	−0·12	0·08	0·19	0·23	0·27	0·30	0·31	0·15
0·698	−0·09	0·09	0·19	0·23	0·27	0·29	0·30	0·15
0·747	−0·06	0·10	0·19	0·23	0·26	0·27	0·29	0·10
0·797	−0·03	0·11	0·19	0·22	0·25	0·26	0·27	0·08
0·848	0	0·11	0·19	0·21	0·23	0·25	0·26	0·04
0·897	+0·03	0·12	0·19	0·21	0·22	0·23	0·23	+0·01
0·948	0·07	0·13	0·18	0·18	0·19	0·21	0·21	−0·06
0·967	0·10	0·15	0·19	0·19	0·19	0·21	0·19	−0·10

TABLE 4

Measured Pressure Coefficients. Ground distance 15 *in.* ($h = 0{\cdot}5$)

Upper surface

x	$\alpha = 0{\cdot}16°$	$\alpha = 3{\cdot}28°$	$\alpha = 5{\cdot}95°$	$\alpha = 7{\cdot}87°$	$\alpha = 8{\cdot}80°$	$\alpha = 9{\cdot}78°$
0	1·00	+0·06	−2·09	−3·15	−5·26	−0·91
0·005	+0·07	−1·43	−3·17	−4·68	−5·65	−1·01
0·007	−0·01	−1·47	−3·09	−4·57	−5·56	−1·01
0·011	−0·14	−1·29	−2·79	−3·49	−3·50	−1·01
0·024	−0·24	−1·09	−1·64	−2·40	−2·74	−1·01
0·047	−0·32	−0·92	−1·46	−1·85	−2·04	−1·01
0·073	−0·35	−0·83	−1·25	−1·54	−1·69	−1·01
0·098	−0·35	−0·76	−1·10	−1·34	−1·45	−1·01
0·148	−0·35	−0·64	−0·91	−1·09	−1·16	−1·01
0·198	−0·36	−0·59	−0·80	−0·94	−1·02	−0·94
0·297	−0·35	−0·51	−0·66	−0·75	−0·80	−0·83
0·348	−0·32	−0·46	−0·57	−0·65	−0·68	−0·81
0·396	−0·30	−0·40	−0·50	−0·56	−0·59	−0·74
0·447	−0·26	−0·34	−0·43	−0·47	−0·50	−0·71
0·497	−0·23	−0·28	−0·36	−0·39	−0·41	−0·68
0·548	−0·16	−0·24	−0·29	−0·32	−0·33	−0·61
0·596	−0·13	−0·20	−0·24	−0·27	−0·28	−0·55
0·647	−0·12	−0·16	−0·20	−0·21	−0·22	−0·49
0·696	−0·08	−0·12	−0·18	−0·15	−0·15	−0·47
0·748	−0·05	−0·11	−0·10	−0·10	−0·10	−0·42
0·795	−0·03	−0·05	−0·05	−0·05	−0·04	−0·38
0·848	+0·01	−0·01	−0·01	0	0	−0·36
0·896	0·02	+0·03	+0·04	+0·06	+0·05	−0·33
0·948	0·05	0·09	0·10	0·11	0·10	−0·28
0·967	0·09	0·11	0·11	0·12	0·11	−0·26
1·000	0·14	0·16	0·16	0·15	0·14	−0·23

TABLE 4—*continued*

Lower surface

x	$\alpha = 0{\cdot}16°$	$\alpha = 3{\cdot}28°$	$\alpha = 5{\cdot}95°$	$\alpha = 7{\cdot}87°$	$\alpha = 8{\cdot}80°$	$\alpha = 9{\cdot}78°$
0·006	0·33	0·97	0·89	0·49	0·21	0·89
0·007	0·19	0·92	0·97	0·72	0·52	0·95
0·014	+0·07	0·81	1·00	0·94	0·83	0·99
0·026	−0·09	0·58	0·90	0·99	1·00	0·94
0·050	−0·20	0·34	0·69	0·84	0·89	0·73
0·075	−0·26	0·23	0·56	0·72	0·78	0·65
0·100	−0·28	0·16	0·40	0·63	0·70	0·57
0·149	−0·31	0·07	0·35	0·50	0·56	0·44
0·200	−0·33	+0·02	0·26	0·42	0·48	0·37
0·298	−0·34	−0·06	0·17	0·29	0·35	0·24
0·348	−0·32	−0·06	0·15	0·27	0·32	0·21
0·398	−0·29	−0·05	0·14	0·25	0·30	0·19
0·448	−0·26	−0·05	0·14	0·24	0·28	0·15
0·498	−0·23	−0·03	0·13	0·23	0·27	0·15
0·548	−0·20	−0·01	0·13	0·22	0·26	0·13
0·599	−0·15	0	0·13	0·21	0·25	0·11
0·647	−0·11	+0·01	0·14	0·21	0·25	0·10
0·698	−0·09	0·04	0·14	0·21	0·24	0·10
0·747	−0·05	0·05	0·14	0·21	0·24	0·08
0·797	−0·03	0·07	0·15	0·21	0·23	0·05
0·848	0	0·09	0·15	0·20	0·21	+0·01
0·897	+0·03	0·10	0·15	0·19	0·22	0
0·948	0·07	0·12	0·15	0·17	0·18	−0·07
0·967	0·10	0·13	0·15	0·18	0·17	−0·09

TABLE 5

Coefficients of Normal Force, Tangential Force, Lift, Drag and Pitching Moment, from Integrated Experimental Pressure Distributions

(*a*) Ground distance 7 in.; $h = 0{\cdot}23$

α (deg)	C_N	C_T	C_L	C_D	C_m
0·25	−0·074	0·001	−0·074	−0·001	+0·019
3·81	+0·518	0·030	+0·519	+0·004	−0·007
*5·43	0·752	0·069	0·756	+0·002	−0·021
*6·69	0·959	0·128	0·968	−0·015	−0·032
*6·93	0·930	+0·066	0·931	+0·046	−0·020
*9·21	0·824	−0·033	0·809	0·165	−0·117

* For $\alpha > 4°$, the boundary layer on the ground appeared to have separated, and these results are therefore unreliable.

(*b*) Ground distance 11 in.; $h = 0{\cdot}37$

α (deg)	C_N	C_T	C_L	C_D	C_m
0·20	−0·008	0	−0·008	0	+0·012
4·02	+0·510	0·037	+0·511	−0·001	−0·007
5·87	0·716	0·070	0·719	+0·004	−0·012
6·79	0·820	0·094	0·826	0·003	−0·020
7·71	0·908	0·118	0·915	0·005	−0·019
8·17	0·934	0·130	0·943	0·004	−0·018
8·63	0·990	0·142	1·003	0·009	−0·024
9·10	0·742	0·028	0·737	0·089	−0·021

(*c*) Ground distance 15 in.; $h = 0{\cdot}50$

α (deg)	C_N	C_T	C_L	C_D	C_m
0·16	0·016	0	0·016	0	+0·003
3·28	0·401	0·022	0·402	0·001	−0·002
5·95	0·688	0·070	0·692	0·002	−0·011
7·87	0·877	0·117	0·885	0·004	−0·013
8·80	0·959	0·141	0·970	0·007	−0·015
9·78	0·874	0·001	0·861	0·147	−0·084

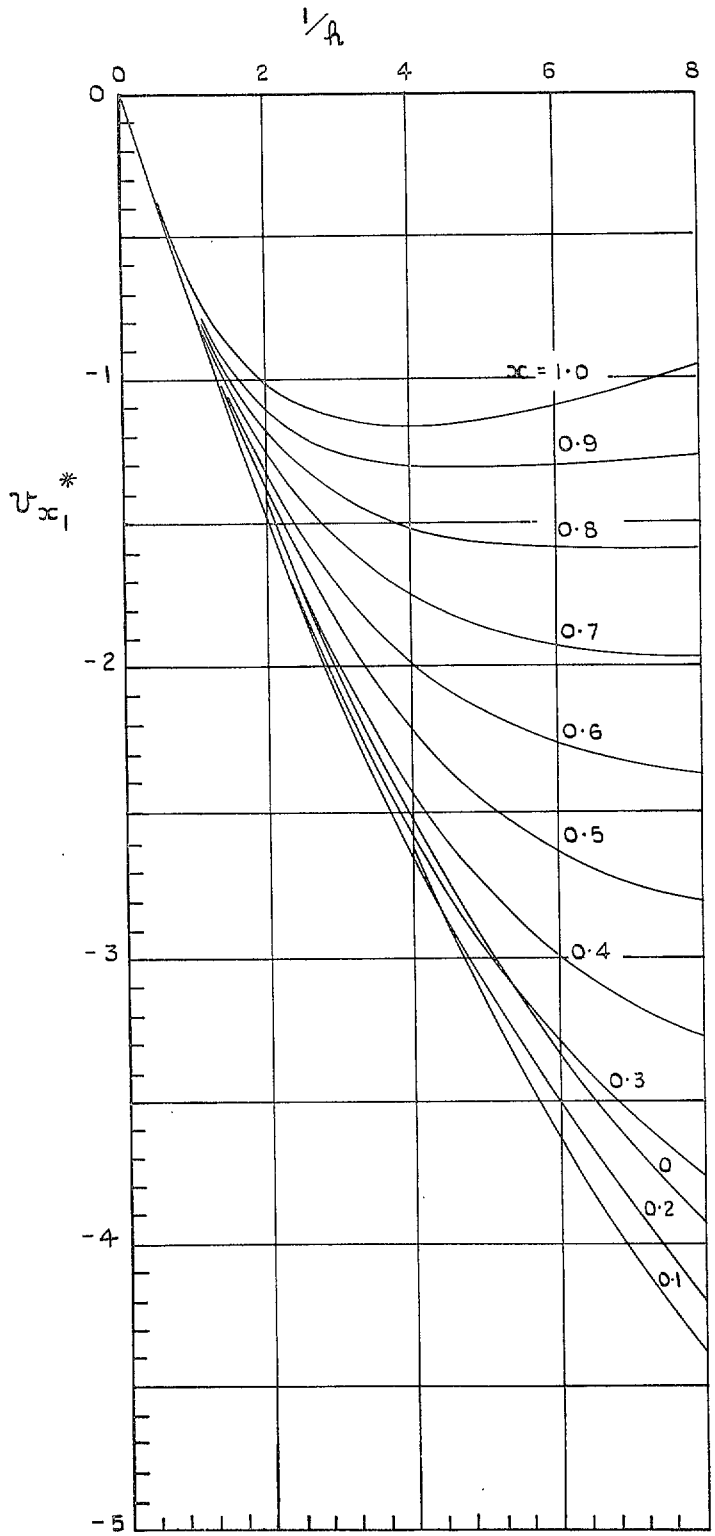

FIG. 1. Chordwise velocity increments due to $\gamma_1(x)$.

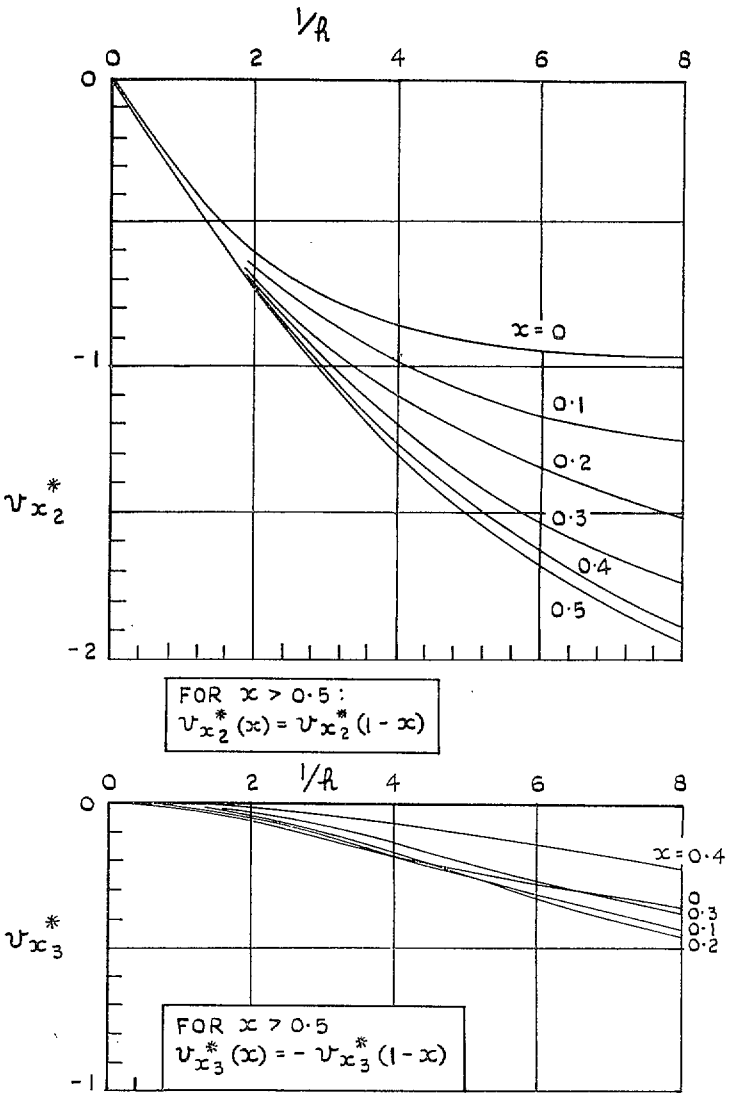

FIG. 2. Chordwise velocity increments due to $\gamma_2(x)$ and $\gamma_3(x)$.

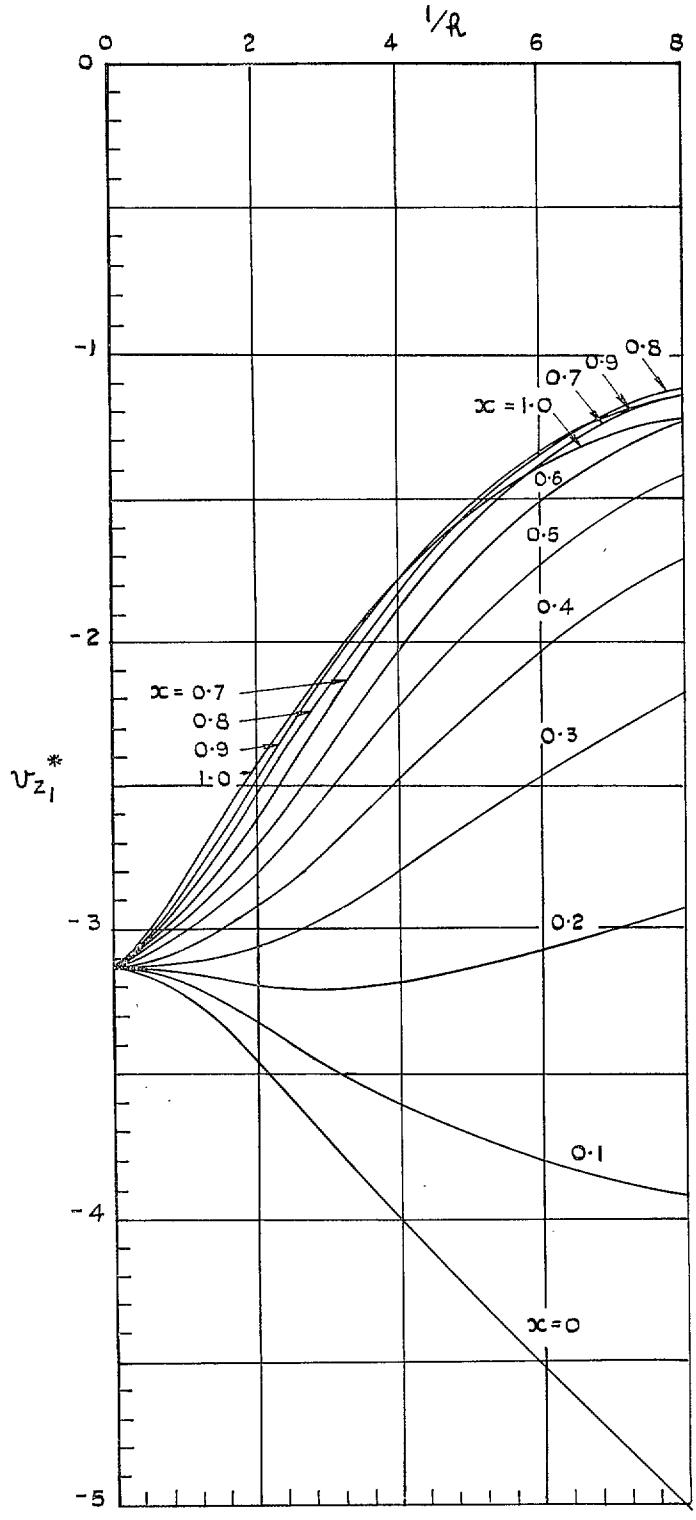

FIG. 3. Vertical velocity increments due to $\gamma_1(x)$.

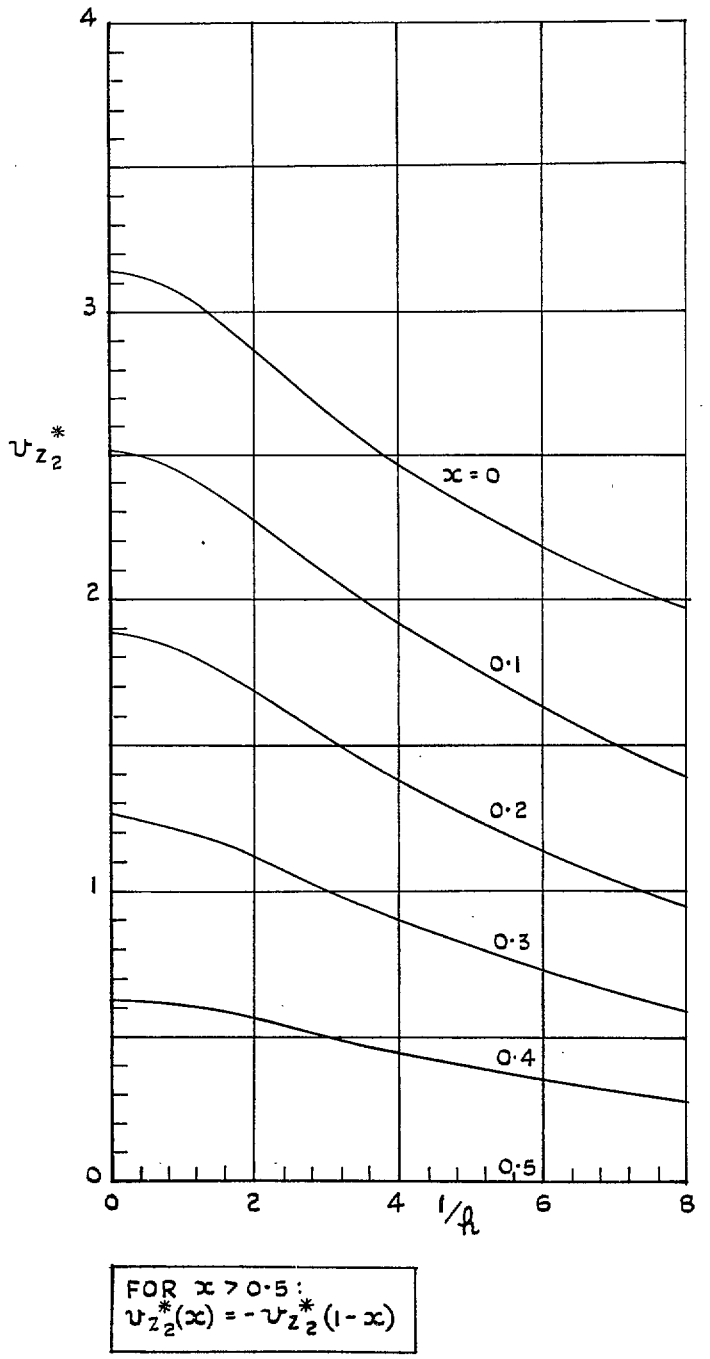

FIG. 4. Vertical velocity increments due to $\gamma_2(x)$.

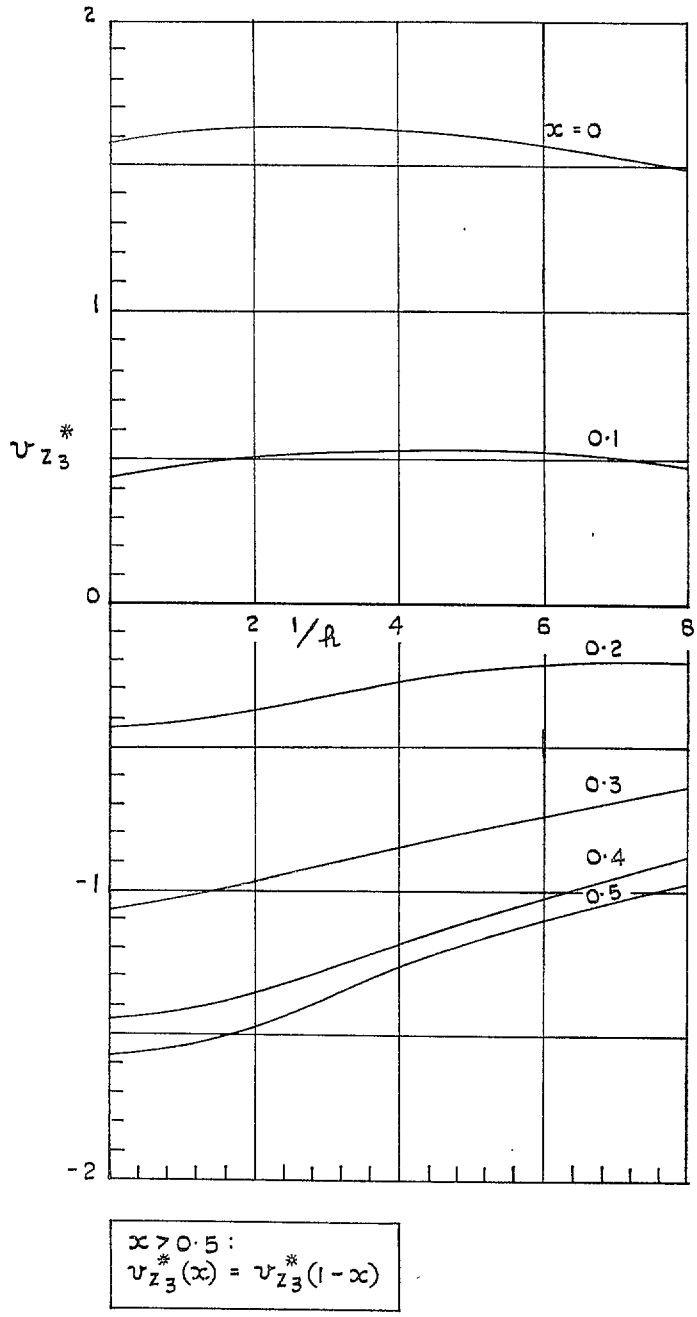

FIG. 5. Vertical velocity increments due to $\gamma_3(x)$.

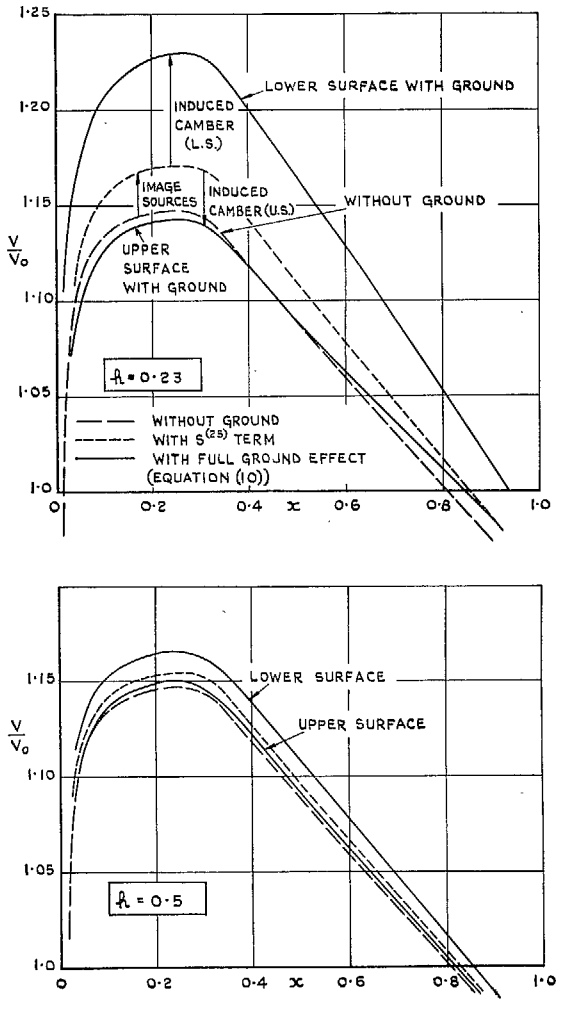

FIG. 6. Calculated velocity distributions at zero incidence on 10 per cent thick RAE 101 wing near the ground.

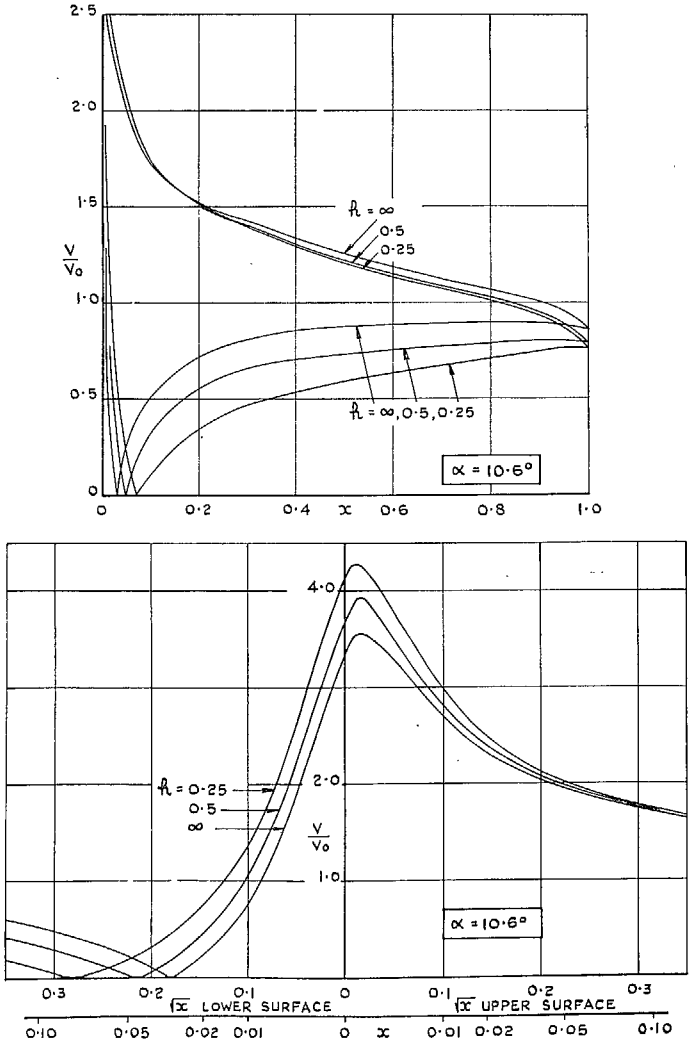

FIG. 7. Calculated velocity distributions on 10 per cent thick RAE 101 wing at $\alpha = 10{\cdot}6$ deg near the ground.

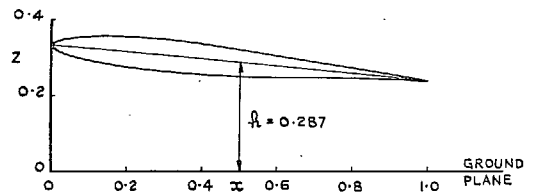

(a). AEROFOIL IN RELATION TO GROUND.

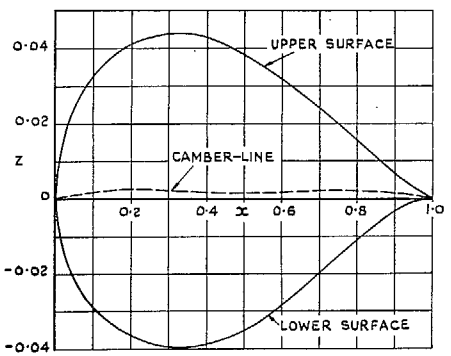

(b). AEROFOIL SECTION.

FIG. 8. Aerofoil 'A' considered by Tomotika (Ref. 10).

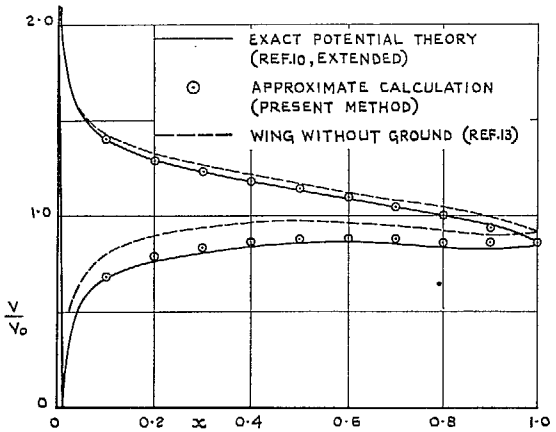

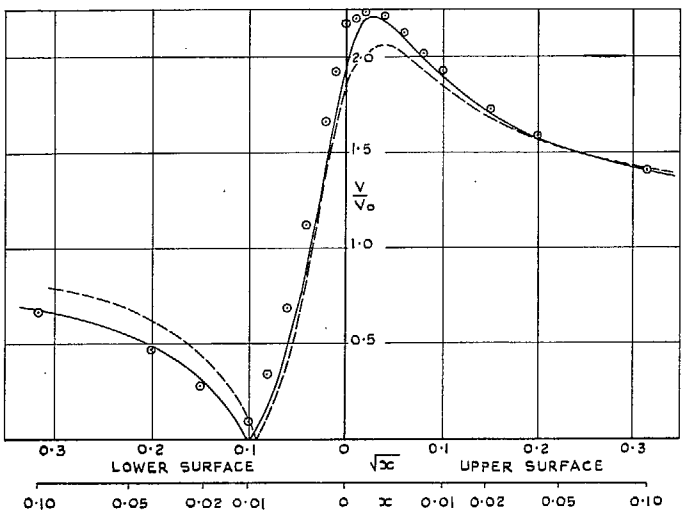

FIG. 9. Comparison of 'exact' and approximate calculated velocities on Tomotika's aerofoil 'A'.

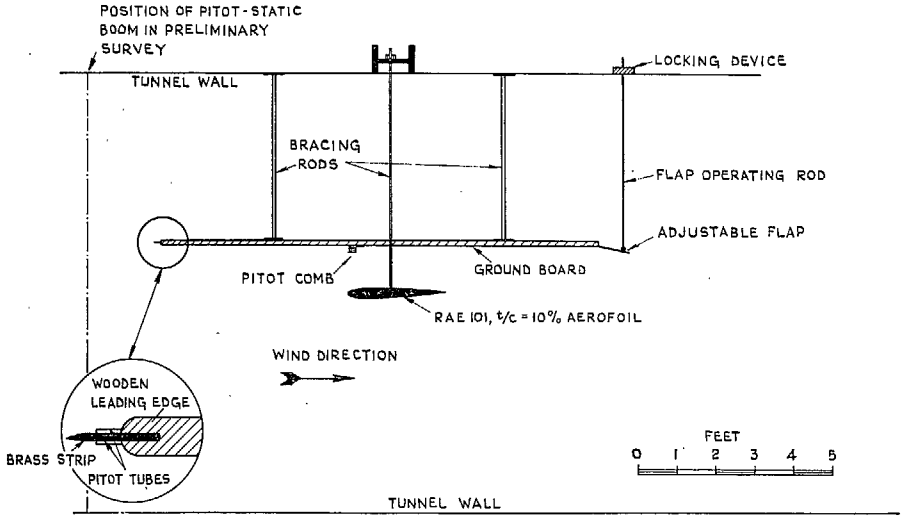

FIG. 10. Sketch of tunnel rig used in experimental investigation.

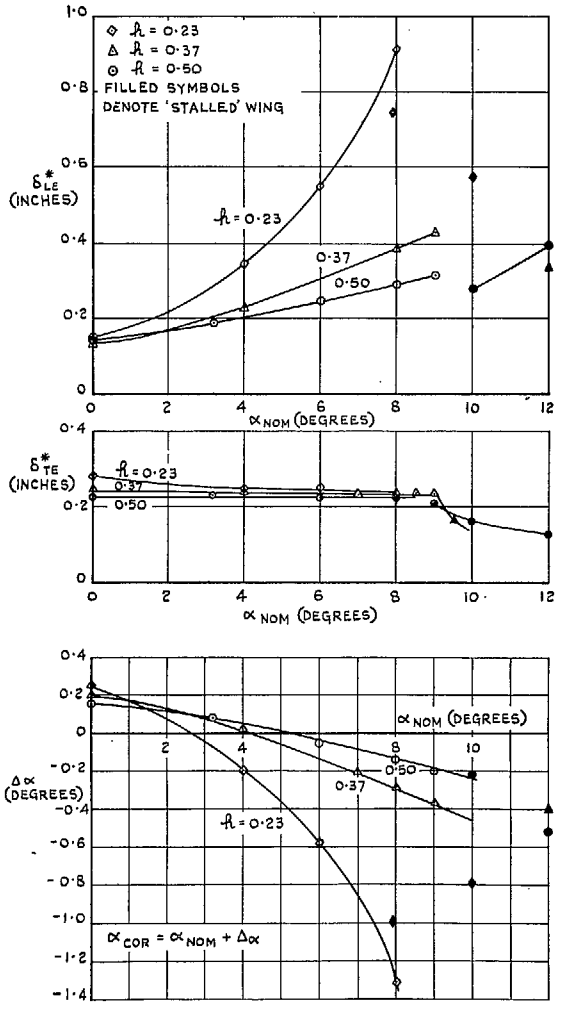

FIG. 11. Measured boundary layer on ground board, and corresponding incidence correction.

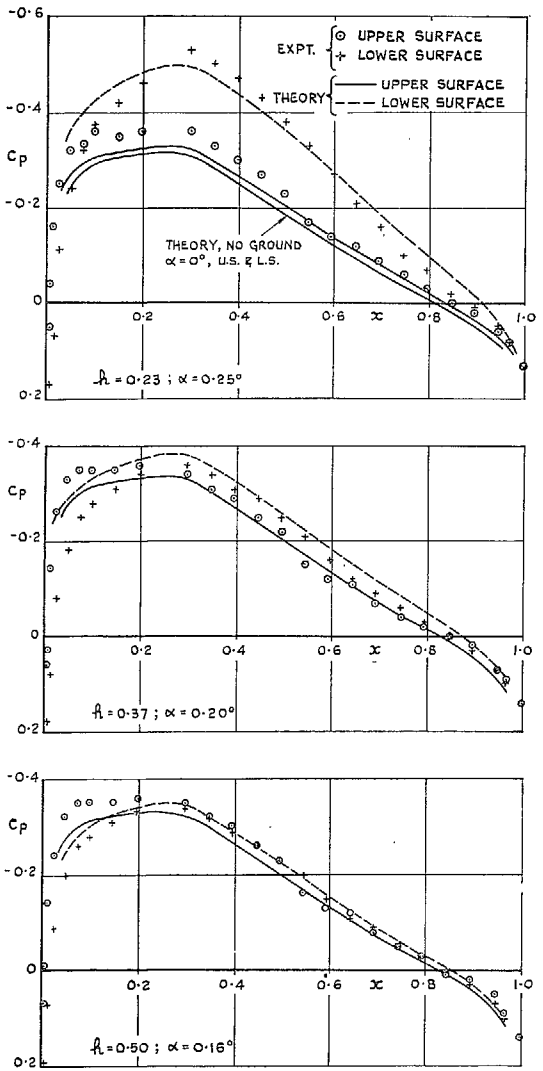

FIG. 12. Theoretical and experimental pressure distributions near zero incidence.

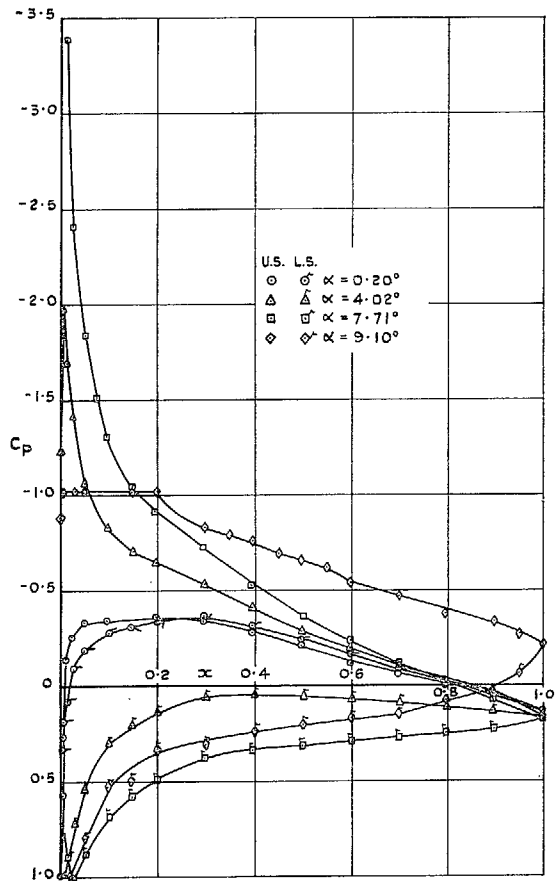

FIG. 13. Experimental pressure distributions, at ground distance $h = 0{\cdot}37$.

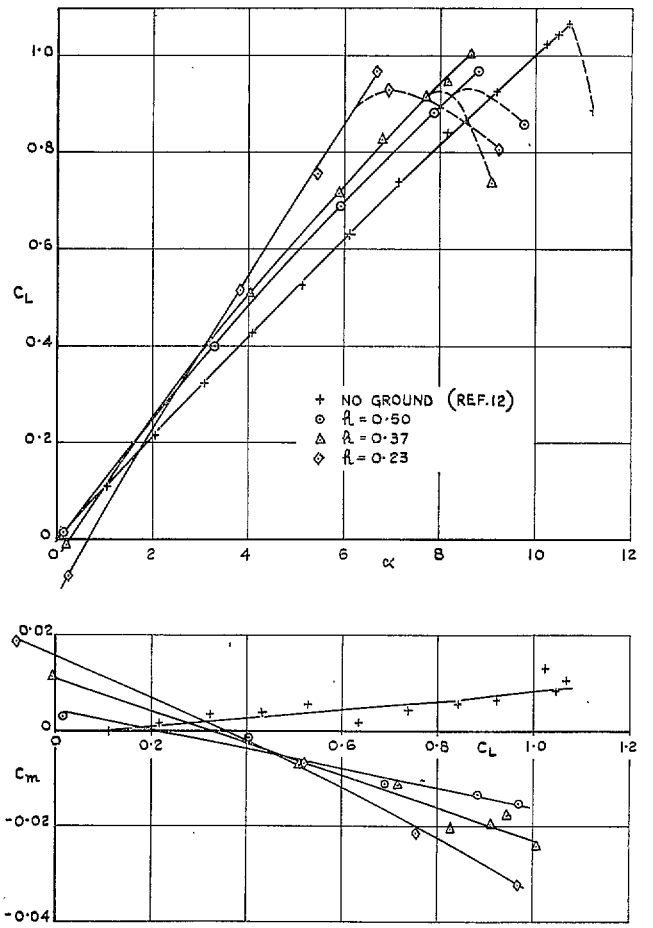

FIG. 14. Measured lift and pitching moment on wing near the ground.

(83081) Wt. 67/1876 K. 5 12/61 Hw.

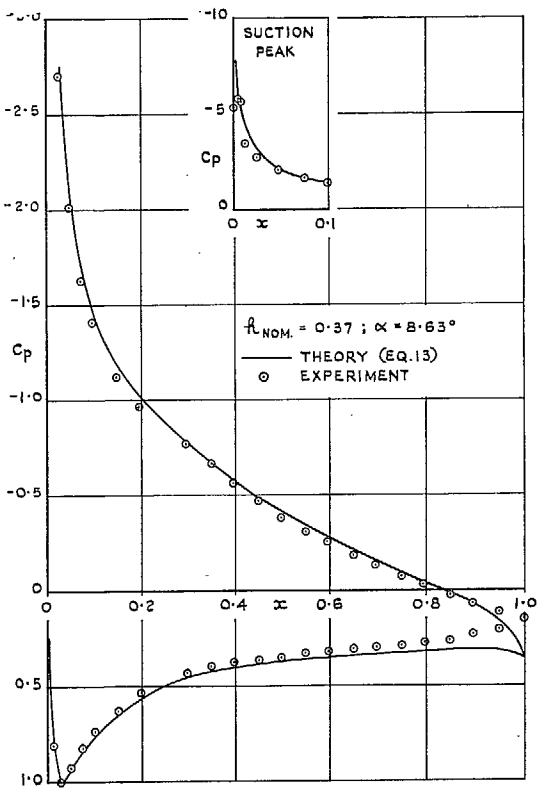

FIG. 15. Theoretical and experimental pressure distributions at $\alpha = 8{\cdot}63$ deg, ground distance $h = 0{\cdot}37$.

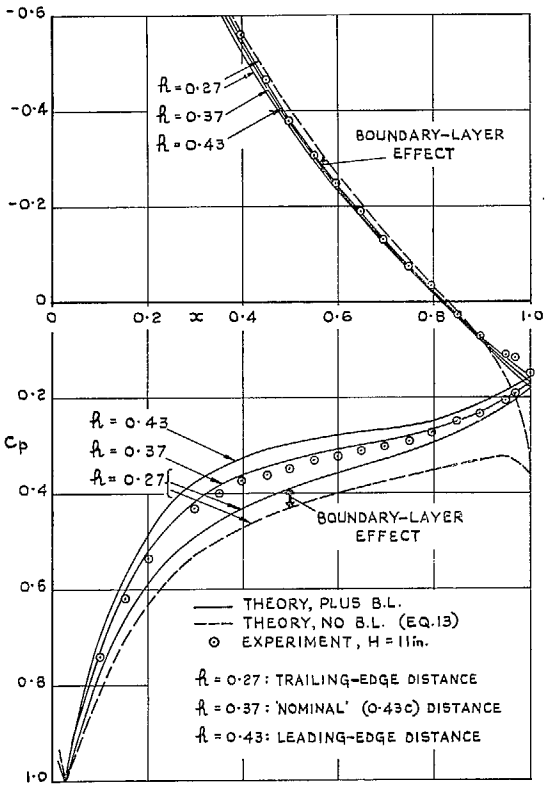

FIG. 16. Theoretical and experimental pressure distributions at $\alpha = 8{\cdot}63$ deg, ground distance $H = 11$ in.

Publications of the Aeronautical Research Council

ANNUAL TECHNICAL REPORTS OF THE AERONAUTICAL RESEARCH COUNCIL (BOUND VOLUMES)

1941 Aero and Hydrodynamics, Aerofoils, Airscrews, Engines, Flutter, Stability and Control, Structures. 63*s.* (post 2*s.* 3*d.*)

1942 Vol. I. Aero and Hydrodynamics, Aerofoils, Airscrews, Engines. 75*s.* (post 2*s.* 3*d.*)
Vol. II. Noise, Parachutes, Stability and Control, Structures, Vibration, Wind Tunnels. 47*s.* 6*d.* (post 1*s.* 9*d.*)

1943 Vol. I. Aerodynamics, Aerofoils, Airscrews. 80*s.* (post 2*s.*)
Vol. II. Engines, Flutter, Materials, Parachutes, Performance, Stability and Control, Structures. 90*s.* (post 2*s.* 3*d.*)

1944 Vol. I. Aero and Hydrodynamics, Aerofoils, Aircraft, Airscrews, Controls. 84*s.* (post 2*s.* 6*d.*)
Vol. II. Flutter and Vibration, Materials, Miscellaneous, Navigation, Parachutes, Performance, Plates and Panels, Stability, Structures, Test Equipment, Wind Tunnels. 84*s.* (post 2*s.* 6*d.*)

1945 Vol. I. Aero and Hydrodynamics, Aerofoils. 130*s.* (post 3*s.*)
Vol. II. Aircraft, Airscrews, Controls. 130*s.* (post 3*s.*)
Vol. III. Flutter and Vibration, Instruments, Miscellaneous, Parachutes, Plates and Panels, Propulsion. 130*s.* (post 2*s.* 9*d.*)
Vol. IV. Stability, Structures, Wind Tunnels, Wind Tunnel Technique. 130*s.* (post 2*s.* 9*d.*)

1946 Vol. I. Accidents, Aerodynamics, Aerofoils and Hydrofoils. 168*s.* (post 3*s.* 3*d.*)
Vol. II. Airscrews, Cabin Cooling, Chemical Hazards, Controls, Flames, Flutter, Helicopters, Instruments and Instrumentation, Interference, Jets, Miscellaneous, Parachutes. 168*s.* (post 2*s.* 9*d.*)
Vol. III. Performance, Propulsion, Seaplanes, Stability, Structures, Wind Tunnels. 168*s.* (post 3*s.*)

1947 Vol. I. Aerodynamics, Aerofoils, Aircraft. 168*s.* (post 3*s.* 3*d.*)
Vol. II. Airscrews and Rotors, Controls, Flutter, Materials, Miscellaneous, Parachutes, Propulsion, Seaplanes, Stability, Structures, Take-off and Landing. 168*s.* (post 3*s.* 3*d.*)

Special Volumes

Vol. I. Aero and Hydrodynamics, Aerofoils, Controls, Flutter, Kites, Parachutes, Performance, Propulsion, Stability. 126*s.* (post 2*s.* 6*d.*)
Vol. II. Aero and Hydrodynamics, Aerofoils, Airscrews, Controls, Flutter, Materials, Miscellaneous, Parachutes, Propulsion, Stability, Structures. 147*s.* (post 2*s.* 6*d.*)
Vol. III. Aero and Hydrodynamics, Aerofoils, Airscrews, Controls, Flutter, Kites, Miscellaneous, Parachutes, Propulsion, Seaplanes, Stability, Structures, Test Equipment. 189*s.* (post 3*s.* 3*d.*)

Reviews of the Aeronautical Research Council

1939–48 3*s.* (post 5*d.*) 1949–54 5*s.* (post 5*d.*)

Index to all Reports and Memoranda published in the Annual Technical Reports

1909–1947 R. & M. 2600 6*s.* (post 2*d.*)

Indexes to the Reports and Memoranda of the Aeronautical Research Council

Between Nos. 2351–2449	R. & M. No. 2450 2*s.* (post 2*d.*)
Between Nos. 2451–2549	R. & M. No. 2550 2*s.* 6*d.* (post 2*d.*)
Between Nos. 2551–2649	R. & M. No. 2650 2*s.* 6*d.* (post 2*d.*)
Between Nos. 2651–2749	R. & M. No. 2750 2*s.* 6*d.* (post 2*d.*)
Between Nos. 2751–2849	R. & M. No. 2850 2*s.* 6*d.* (post 2*d.*)
Between Nos. 2851–2949	R. & M. No. 2950 3*s.* (post 2*d.*)
Between Nos. 2951–3049	R. & M. No. 3050 3*s.* 6*d.* (post 2*d.*)

HER MAJESTY'S STATIONERY OFFICE

from the addresses overleaf

Printed and published by
HER MAJESTY'S STATIONERY OFFICE

To be purchased from
York House, Kingsway, London W.C.2
423 Oxford Street, London W.1
13A Castle Street, Edinburgh 2
109 St. Mary Street, Cardiff
39 King Street, Manchester 2
50 Fairfax Street, Bristol 1
35 Smallbrook, Ringway, Birmingham 5
80 Chichester Street, Belfast 1
or through any bookseller

Printed in England

S.O. Code No. 23-3238